## Quantitative Phase Microscopy for the evaluation and prediction of Mesenchymal Stromal Cell osteogenesis

By Joseph Selorm Ametepe

(Under the Direction of Luke J Mortensen)

#### Abstract

FDA-approved mesenchymal stromal cell (MSC) clinical therapies have been elusive despite strong evidence of their applications in regenerative medicine due to their potential for multi-lineage differentiation, immunomodulation, and paracrine factor secretion. MSCs can provide regenerative potential to areas of the body such as tendons, ligaments, cartilage, and bone. A major hurdle in translation is determining cell quality during expansion and biomanufacturing, so methods that can robustly and non-destructively evaluate their performance will significantly advance this field. With the development of advanced imaging-based techniques to access high-dimensional morphological analysis, we investigated short-term morphological profiles of MSCs correlated with long-term osteogenic differentiation. Using label-free phase imaging, we captured features like GLCM contrast and correlation that tracked differentiation over time. UMAP confirmed visual trends, and random forest models successfully predicted day 28

mineralization from early features. These findings lay the groundwork for future in-line monitoring and selection of high-performance MSC cultures during manufacturing.

**Keywords:** Mesenchymal Stromal Cells, label-free, Quantitative phase imaging, Differentiation potential, high-dimensional morphological analysis, Differential Phase contrast imaging

## Quantitative Phase Microscopy for the evaluation and prediction of Mesenchymal Stromal Cell osteogenesis

by

Joseph Selorm Ametepe

B.S. Georgia Gwinnett College, 2019

A Thesis Submitted to the Graduate Faculty of The University of Georgia in Partial Fulfillment of the Requirements for the Degree

MASTER OF SCIENCE

ATHENS, GEORGIA

2025

## © 2025

Joseph Selorm Ametepe

All Rights Reserved

# Quantitative Phase Microscopy for the evaluation and prediction of Mesenchymal Stromal Cell osteogenesis

## by

## JOSEPH SELORM AMETEPE

Major Professor: Luke J Mortensen

Committee: Cheryl Gomillion

Ross Marklein S

Electronic Version Approved: Ron Walcott Vice Provost for Graduate Education and Dean of the Graduate School The University of Georgia May 2025

#### **ACKNOWLEDGEMENTS**

I would like to take some time to give some thanks for everyone that has supported me during this entire process. I want to first thank Professor Luke Mortensen for having the patience and care to help me along this process of getting my degree. He has been a great mentor and pushed me when I needed the push. I would also like to thank my committee members for all their valuable feedback and patience. I would also like to thank my dad Joseph Divine Ametepe who has always had my back and motivated me no matter what challenges I faced.

Furthermore, I would like to thank all my friends and family who have been there cheering me on as I complete my master's program. They have been great positivity when needed during the harder times of this process. I would also like to thank God for giving me the strength and perseverance to push through all the ups and downs that come with lab work and allowing me to have the strength and determination to push on through. This has been a great experience and I look forward to seeing where this takes me.

Go Georgia Bulldogs!!

iv

## TABLE OF CONTENTS

	F	Page
Acknowled	gments	. iv
List of Tabl	les	vii
List of Figu	ires.	viii
CHAPTER	1: Literature Review.	1
1.1.	Mesenchymal Stromal Cells Background.	1
1.2.	Historical Background of Cell Culture.	3
1.3.	Differentiation Process.	8
1.4.	Phase Microscopy.	11
1.5.	Clinical Trials.	14
1.6.	Gray Level Co-occurrence Matrix (GLCM).	18
1.7.	ALP and Alizarin Red Staining.	22
CHAPTER	2: Experimental Design and Methods.	24
2.1.	Cell Culture.	24
2.2.	Image Collection.	26

	2.3.	Alizarin Red Staining and Quantification.	. 27
	2.4.	Alkaline Phosphate (ALP) Activity Assay.	27
	2.5.	GLCM Evaluation.	. 28
	2.6.	Statistical Method.	. 28
СНАР	TER	3: Results.	.30
	3.1.	Alizarin Red Staining.	30
	3.2.	ALP Activity for all Cell Lines across days.	.33
	3.3.	Differential Phase Contrast Imaging over the differentiation process.	34
	3.4.	Mean Intensity across days for all cell lines.	37
	3.5.	Gray Level Co-occurrence Matrix (GLCM).	. 38
	3.6.	Uniform Manifold Approximation and Projection (UMAP) space	42
	3.7.	Phase as a measure of differentiation progress.	. 43
	3.8.	Phase imaging to predict early detection differentiation potential.	43
СНАР	TER	4: Discussion.	47
	4.1.	Alizarin red and ALP.	47
	4.2	Mean intensity and cellular secretion.	48
	4.3.	GLCM characterization.	.48

4.4.	UMAP visualization correlated with GLCM.	50
4.5.	Random forest model and machine learning.	50
4.6.	Model validation.	51
CHA	APTER 5: Conclusion	53
REF	TERENCES	55

## LIST OF TABLES

	Page
Table 1: Historical timeline of the development of Mesenchymal Stromal Cells (MSCs)	
research	6
Table 2: MSC Clinical Trial Phases.	15
Table 3: Specifications of cells used in Experiment	23
Table 4: Labeling of the four 24-well plates (microplates)	24
Table 5: p-value interpretation	28

## LIST OF FIGURES

Pag	зe
Figure 1.1.1: Mesenchymal stromal cells (MSCs) in-vitro differentiation	
Figure 1.1.2: MSCs as important therapeutic tool for the treatment of a variety of diseases2	
Figure 1.3.1: Arrangement of the parts of the phase contrast microscopy starting from the light	
source to the image plane (reference)	
Figure 1.4.1: Statistics of registered clinical trials using MSCs and sources in which MSCs are	
used in clinical trials	
Figure 3.1.1: Comparison of the Alizarin red staining over 28 days for 3 MSC donors (RB183,	
RB71, and RB175)	0
Figure 3.1.2: Alizarin Red Trends for all five cell lines from day 7 through day 28	l
Figure 3.2.3: Area under the curve for RB71, RB175, RB177, RB277, and RB183 through day	
28	32
Figure 3.2.1: ALP Activity for cell lines for RB183, RB71, RB175, RB177, and RB277 across	
Days	
Figure 3.3.1: Normalized gray scale DPC images over 28 days for the MSC donors (RB183,	
RB177, RB277, RB71, and RB175)	4
Figure 3.3.2: Grayscale images of RB183 on Day 7 vs Day 28. with a small zoomed in section of	of
the 24 well plate.	5

Figure 3.3.3: RB183 Day 7 vs Day 28 shows the progression of mineral deposits and extra
cellular matrix from Day 7 to Day 28
Figure 3.4.1: Biological replicates line graphs over time for the various cell lines across days 7,
14, 21, and 28
Figure 3.4.2: Mean Intensity Line graphs for RB175, RB177, RB183, RB277, and RB71 across
days 7, 14, 21, and 2838
Figure 3.5.1: A visualization of the sample spliced images of the montaged timepoints are shown
below with a clear increase in mineralization over a 28-day period
Figure 3.5.2: The averaged homogeneity for RB183 over 28 days shows a gradual decrease over
time
Figure 3.5.3: The correlation of the image shows a quick decrease to steady state over 28 days
with no clear difference between the days
3.5.4: The averaged contrast for RB183 over 28 days; the various time points differ with Day 28
having the highest contrast and day 7 having the lowest initial contrast40
Figure 3.5.5: The averaged energy for RB183 over 28 days; donor at day 7 is highest with a
steady decline to day 28 days of differentiation
Figure 3.5.6: The averaged dissimilarity for RB183 over 28 days; differentiation is highest
around day 28 and lowest around day 7 for the donor
Figure 3.6.1: Combined UMAP dimensionality reduction for all cell lines (RB175, RB177,
RB183, RB277, and RB71)

Figure 3.6.2: Showing a UMAP visual representation of trendlines seen in the GLCM graphs in
the previous section for each of the GLCM features
Figure 3.7.1 Shows the correlation between the phase features as well as Alizarin red value for
each day for all cell lines44
Figure 3.8.1: Random Forest Regression and feature Importance driving the regression line for
Day 28 AUC (Day 7)44
Figure 3.8.2: Random Forest Regression and feature Importance driving the regression line for
Day 28 AUC (Day 14)45
Figure 3.8.3: Random Forest Regression and feature Importance driving the regression line for
Day 28 AUC (Day 21)45
Figure 3.8.4: Random Forest Regression and feature Importance driving the regression line for
Day 28 AUC (Day 28)46
Figure 3.8.5: 5-fold cross validation R <sup>2</sup> scores with significance between days

## **CHAPTER 1:**

#### LITERATURE REVIEW

## 1.1 Mesenchymal Stromal Cells Background

Found in almost all tissues, Mesenchymal Stromal Cells (MSCs) are a subset of heterogeneous non-hematopoietic fibroblast-like cells. As depicted in figure 1, MSCs can differentiate into important lineage under defined conditions in vitro and in limited situations after implantation in vivo<sup>1</sup>.

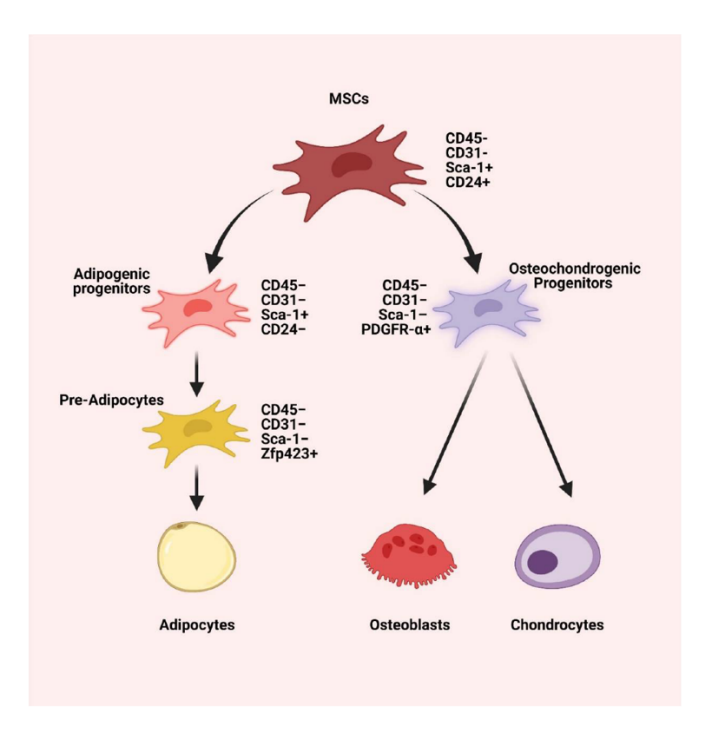


Figure 1.1.1: Mesenchymal stromal cell (MSC) differentiation into osteoblasts, adipocytes, and chondrocytes<sup>1,69</sup>

Specifically, MSCs can differentiate into bone cells, cartilage cells, and fat cells; and have the potential to help repair and regenerate tissues, and modulate the immune response<sup>2, 3, 69</sup>. Because of MSC ability to differentiate and modulate immune response, they have been investigated as therapeutics in areas such as tissue regeneration, immune diseases, and similar application areas (Figure 2) <sup>2, 4, 5</sup>.

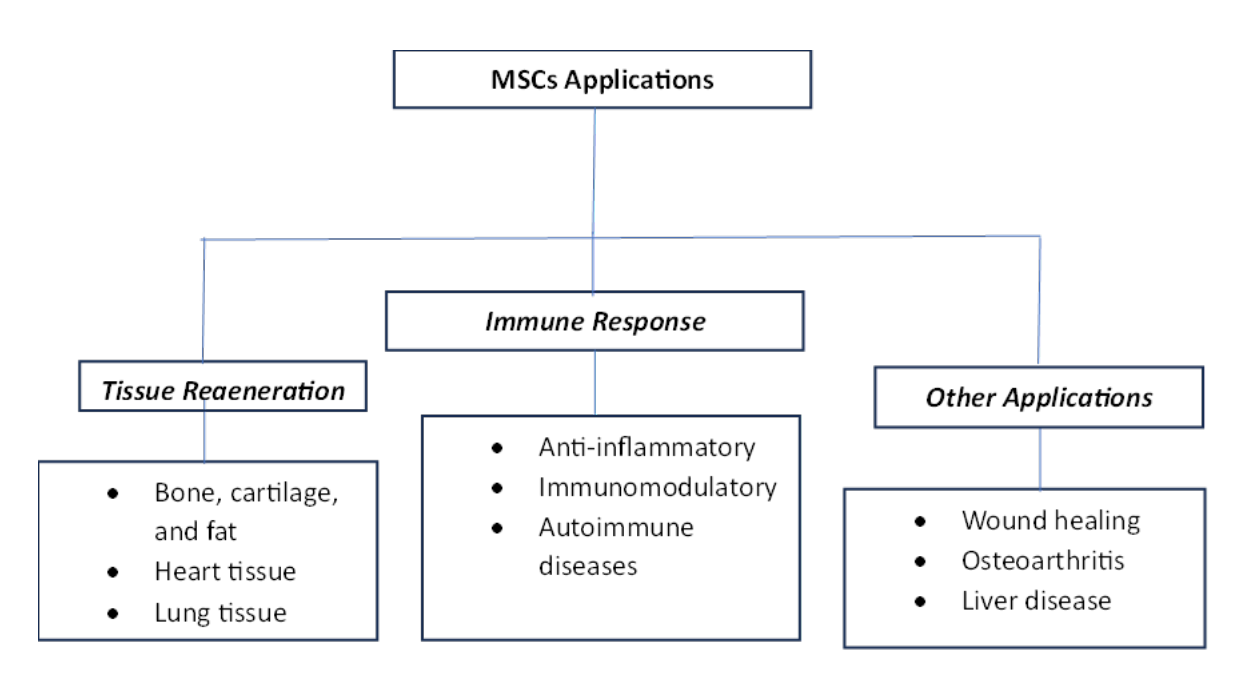


Figure 1.1.2: MSCs as important therapeutic tool for treatment of variety of diseases such as tissue generation, immune response, and other applications.

For tissue regeneration applications, MSCs can differentiate into bone, cartilage, and fat cells, which are important for skeletal structure<sup>2</sup>; can help repair lung tissue in chronic obstructive pulmonary disease<sup>3,4</sup>; and can help repair damaged nerve tissue in the spinal cord<sup>4,54</sup>. For immune applications, MSCs release immune modulatory factors <sup>56</sup> and interact directly with

immune cells <sup>55</sup>. For contact-mediated mechanisms, MSCs interact directly with immune cells including T cells, B cells, dendritic cells or DCs, and macrophages to influence their behavior through anti-inflammatory cytokines some being Interleukin-10 (IL-10), Interleukin-4 (IL-4), Indoleamine 2,3-Dioxygenase (IDO) and Transforming Growth factor Beta (TGF-Beta). MSCs also have adhesive molecules like VCAM-1, ICAM-1, and integrins (e.g., CD44, CD105, CD90, CD1) to facilitate cell-to-cell and cell-matrix interaction<sup>54, 55, 70 - 74</sup>. For paracrine activity, MSCs secrete a range of molecules including cytokines (e.g., Interleukins like IL-1, IL-6, and IL-10; Tumor necrosis factor or TNF; and interferons like IFN-gamma), which play critical roles in regulating immune responses, inflammation, and cell growth; growth factors (e.g., vascular endothelial growth factor, fibroblast growth factor, and hepatocyte growth factor), which promote tissue repair and regeneration; and chemokines, which play a direct role in the movement of white blood cells to sites of inflammation, infection, or tissue damage<sup>54, 55</sup>. MSCs acting as an immunomodulatory agent could assist with treating autoimmune diseases such as lupus and multiple sclerosis<sup>75</sup>. For other applications, MSC can help treat chronic wounds and stimulate healing, reduce inflammation and promote cartilage repair – osteoarthritis, and treat liver diseases like cirrhosis<sup>76-78</sup>.

#### 1.2. Historical background of cell-culture

In order to appreciate advances made in Mesenchymal Stromal Cell (MSC) research, it is important to acknowledge those who performed foundational research. Early researchers like Santiago R. Y. Cajal, Wilhelm Roux, Ross G. Harrison, Montrose Burrows, and Alexis Carrel played a critical role in what would become stem cell research. Cajal's work on cell structure showed that different cells have specialized roles, which was a big step toward understanding

what is now known as stem cells<sup>6</sup>. Cajal was the first to apply silver nitrate to the anatomy of the nervous system. This led to the understanding of the nervous system and establishing that the nerve cell (neuron) is the basic unit of the nervous structure. Cajal used staining technique, now known as the Golgi staining, for the general study the fine structure of the nervous tissues of the brain, sensory centers, and the spinal cords of embryos and young animals<sup>7</sup>. Additionally, he used these nerve specific stains to differentiate neurons from other cells and to trace the structure and connections of the nervous cells in gray matter and spinal cord. During this time period, living cell analyses were limited to embryos developed outside of the adult like frogs, sea urchins, mollusks, and ascidians.

In 1885, Wilhelm Roux suggested that, with the proper conditions, animal cells could survive and be maintained outside the body. He demonstrated this by successfully removing a part of the medullary plate from a chick embryo, which survived for 13 days (about 2 weeks) under a warm saline solution. Roux's experiment established the groundwork for further research in cell culture<sup>8</sup>.

Motivated by Roux's work, Ross G. Harrison successfully cultivated frog nerve tissue outside the body. His work demonstrated that it is possible to grow living tissue in vitro for the first time<sup>9</sup>. This work provided a method to study tissue behavior outside the body opening the door for further research fields like embryology, genetics, virology, and oncology<sup>10, 11</sup>. Learning form Harrison's culture technology, Montrose Burrows and Alexis Carrel succeeded in cultivating explants from dogs, cats, rats, and guinea pigs<sup>12</sup>. Carrel and Burrows extended the field by developing a method for growing tissues outside of a living organism or in vitro. Their technique involved placing small tissue fragments in a nutrient-rich medium (derived from embryonic chicken tissue), which allowed for cell propagation and growth in vitro<sup>12</sup>. This in

vitro technique marked a significant milestone in tissue culture research. Additionally, Carrel et. al., using chick heart tissues showed that cultures survived for much longer than the normal lifespan of the chick. Carrel's team produced and maintained a series of chick heart tissue cultures at the Rockefeller Institute in New York City from 1912 to 1946<sup>13</sup>. During this duration, the series of chick heart tissue cultures, not only remained alive, but also kept dividing. Carrel et. al.'s findings influenced the cell immortality idea and cellular aging from the 1920's to the 1960's<sup>14</sup>. His work hinted that cells might even be able to repair tissues, opening the door to regeneration possibilities. Furthermore, the accumulation of new findings and knowledge made it possible to test the function, potential, and application of cells from many animals, and many tissues, under a variety of conditions.

Albert Claude, using the newfound knowledge, developed a new technique called cell fractionation<sup>15</sup>. Claude's new method allowed for the separation of the various components of cells through differential centrifugation<sup>16, 17</sup>. His work opened the door for scientists to explore the structure, inner workings, and functions of cells and organelles leading to an even deeper understanding of how cells operate. These important foundations, shown in table 1, have played significant roles in establishing what we know today in stem cell research.

Alexander Friedenstein<sup>18, 21</sup> further pushed this discovery through his own experiments; by transplanting various bone marrow cells from different tissues into rats<sup>18, 19</sup>. Through his experiments he was able to observe that fibroblast-like cells in bone marrow had the capabilities of forming colonies in vitro<sup>19</sup>. He also observed a populations of rodent bone marrow cells that were rapidly adherent to plastic, common characteristics still associated with MSCs today. Friedenstein et. al.'s contributions were advanced in the 1990s by Arnold Caplan. Caplan theorized that MSCs had the ability to differentiate into various types of tissues and with

regenerative capabilities. Additionally, Caplan through his work, found that MSCs can (i) modulate the immune systems, (ii) inhibit both programmed cell death and scar formation, (iii) stimulate blood-vessel formation, and (iv) promote the growth of tissue-specific stem cells (somatic or adult stem cells) that are more specialize than embryonic stem cells and can only differentiate into a specific range of cell types within the tissue or organ they reside in 19, 20, 57. Caplan, like Friedenstein, also isolated human MSCs from adult bone marrow, establishing the conceptual and technical foundation for subsequent studies. Caplan coined the term "Mesenchymal Stem Cell" because of the ability of cells to differentiate into multiple types that form connective tissues exhibiting significant regenerative potential 22.

Table 1: Historical timeline of development of Mesenchymal Stromal Cells (MSCs) research.

Authors	Contribution	Importance	Reference	
Santiago R. Y. Cajal (1852 – 1934)	9		doi: 10.1007/s00415017025 5. PMID: 11284138.	
Wilhelm Roux (1850 –1924)	Observation and documentation of tissue culture	Chick embryos survived in warm saline solution	https://www.nobelpr ize.org/prizes/medi cine/1906/article/	
Ross G. Harrison (1870 – 1959)	8		doi:10.3181/00379727- 4-98.	
Montrose Burrows (1884 – 1947) Coined the phrase "tissue culture."		Study of tissues from warm-blooded animals.	doi: 10.1084/jem.13.3.387. PMID: 19867420; PMCID: PMC2125263.	
Alexis Carrel (1873 - 1944)	Immortality of cells	New method of separating cell components	doi: 10.1084/jem.15.5.516 . PMID: 19867545; PMCID: PMC2124948.	

Albert Claude (1898 – 1983)	Cell fractionation or ability of cells to repair tissues	Start of regenerative possibilities	doi: 10.1098/rspb.1954.00 19. PMID: 13167066.	
Alexander Transplanting bone marrow cells from different tissues		Concept to application	https://doi.org/10.111 1/j.1365- 2184.1970.tb00347.x	
Arnold Caplan (1942 – 2024)	Coined MSC	MSCs have regenerative capabilities and can differentiate into various types of tissues.	doi:10.1002/sctm.17- 0051	

MSCs are easily able to be isolated and combined with their ease of expansion make them very useful for in vitro experiments further enhancing their applications like orthopedic injuries, autoimmune diseases, and neurological disorders<sup>23</sup>. Expanding clinical trials continue to reveal new applications, advancing MSCs as a transformative option for previously untreatable conditions like bone defects or disorders<sup>23, 58</sup>. MSCs application in bone regeneration or repair occurs through their ability to differentiate into osteoblasts, which are responsible for bone formation<sup>58</sup>. The next sections will examine the MSCs differentiation process, techniques for studying or visualizing cellular structures, standard imaging processing, and clinical trials.

#### 1.3. Differentiation Process:

Taking a closer look at the various differentiation processes is important in understanding how MSCs function and what is currently being done in terms of their application. MSC differentiation is a detailed multiple step process that gives them their ability to transform into specialized tissue. This process is guided and aided by a mix of factors, including chemical signals, the cellular environment, and physical cues all of which work together to guide them toward specific cell identities. Below is an in-depth look at the primary pathways and key regulatory factors that drive MSC differentiation. MSCs can differentiate into bone cells, chondrocytes and adipocytes through several signaling pathways and transcription factors. MSCs that differentiate into bone cells start initially with the formation of osteoblasts<sup>3</sup>. MSCs are driven by several signaling pathways including WnT, TGF- $\beta$ /BMP, and IGF, which regulate their osteogenesis, differentiation, and tissue regeneration. The Wnt plays the role of bone development, promotes MSC proliferation, self-renewal, and differentiation into osteoblasts, GF- $\beta$ /BMP signaling plays the role of bone formation, differentiation into osteoblasts and regulating bone matrix, and IGF promotes MSC osteogenesis and bone regeneration.

Initiation of this signaling pathway leads to the activation of transcription factors such as Runt-related transcription factor 2 (RUNX2), which is essential for osteoblast differentiation (bone-forming cells)<sup>3.</sup> SP7 (also known as Osterix) is downstream of RUNX2, essential for lineage commitment to the osteoplastic. Next is the pre-osteoblast to the osteoblast, which is the ECM development and ALP activity. Finally (Osteoblast to Osteocyte) is the mineralization and maturation process<sup>3,30</sup>. A few methods used to measure osteogenic differentiation are using ALP activity assays as well as Alizarin red staining.

There are many other signaling molecules that influence osteogenic differentiation; the process by which bone marrow MSCs and osteoprogenitors transform into bone forming cells. One of such are Wnt proteins. Through the Wnt/ $\beta$ -catenin signaling pathway, promotion of osteogenic differentiation is done by enhancing the stability of  $\beta$ -catenin, which works in tandem with RUNX2 to stimulate osteoblastic gene expression<sup>30</sup>. Additionally, environmental cues such as mechanical stress, common in bone formation, activate signaling pathways that encourage MSCs to favor osteogenesis over other pathways<sup>30</sup>.

MSCs can also differentiate into chondrocytes a process called chondrogenesis. Chondrocytes are cells that produce cartilage, through a process driven largely by transforming growth factor-beta (TGF- $\beta$ ) and members of the BMP family. Chondrogenesis is primarily regulated by TGF- $\beta$ 1 and TGF- $\beta$ 3, which activate the SOX9 transcription factor, a master regulator for chondrogenic differentiation. SOX9 upregulates cartilage-specific extracellular matrix proteins like collagen type II and aggrecan, which are crucial for cartilage formation<sup>30, 41</sup>. MSCs require a low-oxygen (hypoxic) environment akin to the environment of cartilage<sup>41</sup>. Under low oxygen conditions Hypoxia-inducible factor 1-alpha (HIF-1 $\alpha$ ) is activated enhancing SOX9 activity and pushing cartilage matrix synthesis<sup>30, 41</sup>.

Adipogenic differentiation, where MSCs become fat-storing adipocytes, is regulated by several transcription factors, with peroxisome proliferator-activated receptor gamma (PPAR $\gamma$ ) being the most critical<sup>38</sup>. Upon stimulation by fatty acids or other lipogenic signals, PPAR $\gamma$  activation leads to the expression of genes involved in lipid uptake and storage, such as adiponectin and lipoprotein lipase<sup>38</sup>. CCAAT/enhancer-binding proteins (C/EBPs), especially C/EBP $\alpha$  and C/EBP $\beta$ , work alongside PPAR $\gamma$  to drive adipogenesis by promoting fat-specific

gene expression. Glucocorticoids and insulin, also promote adipogenic differentiation<sup>38</sup>. Mechanical cues have a low impact on this pathway however it is influenced by the presence of certain adipogenic cytokines like leptin and adiponectin. The microenvironment in which MSCs reside can significantly affect their ability to undergo adipogenesis, as seen in areas of the body with high-fat accumulation.

The "niche" or microenvironment (ECM, nearby cells and physical forces) of MSCs can also play an instrumental role in their differentiation fate<sup>50</sup>. The extracellular matrix (ECM), nearby cells and physical forces can all have an impact on how MSCs will differentiate. If the ECM is too stiff MSCs can differentiate into osteogenic cells while ECM having a less stiff characteristic can lead towards adipogenesis<sup>59</sup>. Differentiation outcomes can also be influenced by cytokines, growth factors, and even the immune cells present in the microenvironment<sup>50</sup>. Mechanical stresses that can induce osteogenic differentiation in MSCs including tensile (stretching) forces, while stresses compressive forces are likely to lead to chondrogenesis<sup>50</sup>. These mechanical forces activate integrin receptors on the surfaces of MSCs that then influence signaling pathways, genes expression profiles and ultimately cell fate<sup>50</sup>.

In general, the MSC differentiation process involves commitment and maturation process. The commitment process is when cells are directed toward a specific lineage (Fig. 1), whereas the maturation is where the progenitor cells are transformed into fully differentiable cells. There are many factors that can affect the differentiation process including growth factors, cytokines, transcription factors, and extracellular matrix molecules. It is important to note that not all MSC differentiation are successful as they can be impacted by age or disease. The next section describes how to monitor morphological changes during MSCs differentiation process.

#### 1.4. Phase Microscopy:

In this thesis, we hypothesize that morphological changes that occur in the MSCs during their differentiation process can be monitored and assessed through a technique called phase microscopy. This technique is sensitive to changes in optical thickness, and so could be useful in situations with high production of differing types of extracellular matrix for classification of MSC transformation into cell types like osteoblasts, chondrocytes or adipocytes without the use of staining<sup>60</sup>.

Phase contrast microscopy (PCM), developed by Dutch physicist Frits Zernike in the 1930s, is an optical technique that enhances contrast in transparent, unstained specimens like living cells, microorganisms and thin tissue slices<sup>27</sup>. This technique works by converting small phase shifts in light passing through the sample into visible amplitude changes or brightness, thereby making it possible to visualize cellular structures that would otherwise be nearly invisible. Generally, unstained living cells do not absorb light well making them almost not visible in bright field microscopy because of minimum differences in the intensity distribution. Dr. Zernike's breakthrough, which earned him the Nobel Prize in 1953, allows phase objects (those that do not absorb much light but slightly alter their phase) to appear with high contrast against a bright background<sup>27,37</sup>. Hence the technique became essential for observing live unstained cells, enabling scientists to study cellular dynamics without the use of chemical staining, which could kill or disturb the cells.

In a phase contrast microscope, two main components work together to create the necessary phase shifts; these are annular diaphragm (or phase ring) in the condenser and the phase plate in the objective lens<sup>40</sup>. Figure 3 below shows the main parts of the microscope<sup>60</sup>.

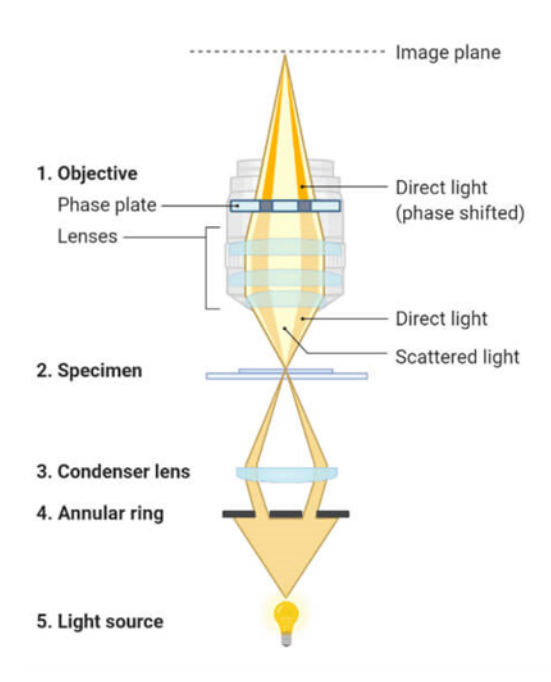


Figure 1.3.1: Arrangement of the parts of the phase contrast microscopy starting from the light source to the image plane<sup>40, 60</sup>.

The microscope consists of a light source, angular ring, condenser lens, specimen stage and objective. The objective contains multiple lenses and a phase plate. Light passing through the annular diaphragm forms a hollow cone that illuminates the sample<sup>27, 29, 43</sup>. When light hits different parts of the sample, some light waves pass through unaffected (direct or diffracted light), while others are scattered by cellular structures (diffracted light)<sup>29, 37, 40</sup>. The direct light remains in phase, while the diffracted light is phase-shifted slightly, typically by about 1.57 radian, due to variations in the samples' refractive index<sup>37</sup>.

Further changes are made to the phase plate in the objective in order to make the phase shifts more visible<sup>29, 37</sup>. The change that is typically made in the phase plate of the objective lens is equivalent to a quarter wavelength ( $\frac{1}{4}$  -  $\lambda$ ) allowing the direct light (un-scattered) to interfere

with the diffracted light, which carries information about the specimen, to cause a ( $\frac{1}{2} - \lambda$ ) phase difference. Such a phase difference can either be constructive or destructive resulting in changes in the amplitude (brightness) of light, which translates into differences in contrast. High contrast images that reveal much of the sample's details are created through the brightening of some areas (constructive interference) and the dimming of others (destructive interference)<sup>39, 37, 40, 43, 43</sup>. Through this techniques it enables either positive or negative phase contrast, depending on the design of the phase plate showing the sample as either lighter or darker against the background<sup>43</sup>.

PCM can be used to assess the differentiation of MSCs in clinical settings due to its ability to allow the visualization of living cells and organelles, that are transparent and colorless, without the need to stain and to study dynamic biological processes like observing living cells in their natural state. Although one drawback in PCM is a halo effect that can occur when a glow appears around a sample's edges losing finer details, there are some correction methods that can be done to limit this unwanted effect<sup>27, 37, 40</sup>.

While PCM is used to visualize cells and cell components, another type of phase contrast microscopy employed to image MSCs is differential phase contrast (DPC). Differential Phase Contrast (DPC) microscopy, is a specialized form of light microscope used to enhance the contrast of weakly absorbing or transparent specimens like mesenchymal stem cells (MSCs), making them more easily visible under a microscope<sup>61</sup>. This enhancement ability is achieved by illuminating the sample at different illumination angles using a programmable LED (low light levels) array minimizing any impact on cell health or biological function. The DPC has an advantage over the standard brightfield microscope because it can detect and visualize minute changes in the phase of light waves that pass through the specimen, which are otherwise

undetectable by a standard brightfield microscope. Additionally, DPC imaging is label free, allowed for the analysis of morphological cell features, and longitudinal live-cell imaging.

The use of the traditional brightfield microscopes to observe transparent and colorless specimens are difficult. Therefore, the use of DPC provides advantages like effective visualization of transparent and colorless specimens, provide enhanced contrast near the edges that surround extended specimen to produce high-contrast images. Additionally, DPC microscopy produces a greater depth of field and can image living cells, tissues, and weakly scattering specimens among other things.

## 1.5. Clinical trials

To understand how and where MSCs are in clinical trials, it is important to discuss the clinical trials in four phases. Phase 1 deals with the safety and assessment of dosage for a new treatment or drug<sup>45</sup>. Often this stage is associated with giving patients different dosages of a treatment. Phase 2 evaluates the effectiveness and safety of the treatment in a larger group of patients<sup>45</sup>. Phase 3 compares the new treatment to standard treatments to confirm its efficacy<sup>45</sup>. Phase 4 the final stage involves studies that look at the long-term effects of a treatment after it has been approved and available for market<sup>45</sup>.

MSCs have garnered a lot of attention due to their versatile regenerative and immunomodulatory potential. Specifically, their ability to treat conditions like osteoarthritis, cardiovascular disease and autoimmune disorders. Although there are potential, clinical outcomes have been slowed due MSC heterogeneity, donor variability and tissue origin, which all affect the consistency in clinical trials<sup>3, 44</sup>. In the United States most clinical trials for MSCs are in phase 1 but the trend has significantly shifted or moved into phase 3. In phase 3, many

clinical trials have been conducted to test the reliability and efficacy of cell therapy. To do so, thousands of patients have received MSC transplants to treat different diseases including Graft versus host disease (GvHD), heart disease, immune system diseases, malignant neoplasms, and neurological disorders. In a phase 3 prospective study of the use of intravenous MSC injection to treat 54 pediatric patients suffering from corticosteroid-resistant acute GvHD, it was reported that the treatment boosted the overall response rate by 28 days compared to the control<sup>63</sup>. Even though GvHD clinical trials span decades, those have led to the development of standardized criteria and Food and Drug Administration (FDA) approved therapies for both acute GvHD and chronic GvHD<sup>64</sup>. Over 79% of the MSC clinical trials are in Phase I and II.

Table 2: MSC clinical trial phases

Early Phase	Phase I	Phase II Phase II	Phase II	Phase III Phase III	Phase III	Phase IV	Not Applicabl e
28	250	341	183	25	31	4	152
2.8%	24.6%	33.2%	18%	2.5%	3.1%	0.39%	15.0%

The table was generated based on data from MSC clinical trial phases<sup>79</sup>.

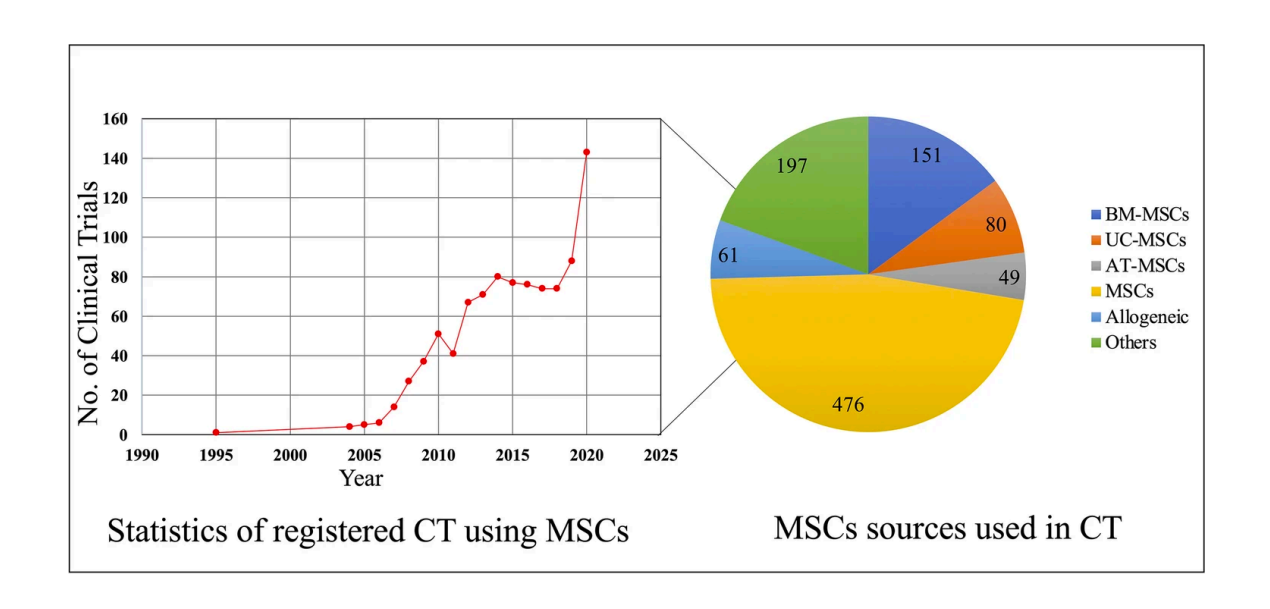


Figure 1.4.1: Statistics of registered CT using MSCs <sup>79</sup>

There have been studies done to look at the preclinical aspects of MSCs as it pertains to in vivo and in vitro. In one study, human bone marrow MSCs were implanted into three biomaterials and cultured for 28 days (about 4 weeks). After this culture period, there were great signs of osteogeneses such as gene expression and mineral deposition<sup>51</sup>. BMSCs are MSCs have been extracted and cultured, and their effects tested in preclinical experiments and thoroughly reviewed in many studies<sup>80-84</sup>. What follows are a few of the preclinical applications and findings. In a systematic infusion of BMSCs study, three patients of ages ranging from 13 to 32 months, received 5.7 to 7.5 × 10<sup>8</sup> cell/kg unmanipulated nucleated cells from siblings. The treatment increased the total body bone mineral content and growth velocity of the patients<sup>82</sup>. In a case-control study, the treatment group had a significantly higher body length increase than the control group and had similar rates of bone mineral content gain with weight-matched healthy children<sup>82</sup>. In another study, two patients had different conditions (aGvHD and transient

pulmonary insufficiency and a bifrontal hygroma), which resolved uneventfully<sup>83</sup>. Another case-control study involving six patients of ages ranging from 2 to 4 years received *ex vivo* expanded autologous BMSCs. Five out of the six patients had significant improvement in growth velocity, one having substantially increased bone mineral content, and one had a urticarial rash that resolved after treatment<sup>83,84</sup>

There are several biomaterial MSC in vivo successful studies, prompting for these biomaterial constructs to be moved to in vivo models. When this was done the results diverged greatly from the osteogenic results that were done in vitro<sup>51</sup>. This drawback highlights the struggle of translating results that are seen in vitro to in vivo experiments. More complex methods such as imaging or machine learning may help bridge this gap and align better with clinical outcomes<sup>51</sup>.

In another study, a young patient received osteoblasts from the father resulting in significant bone mineralization allowing osteoblasts to be more active than before<sup>35</sup>. Another case where a child with hypophosphatasia received a bone marrow transplant from a sibling significantly increased her bone deterioration<sup>52</sup>. Some osteoinduction (OI) have included non-union fractures as well as periodontal regeneration. These differing results points to the idea that if there was a way to predict the success of an MSCs therapy prior to administration of the cells, patient outcomes could be improved<sup>52</sup>. Also, because MSCs have the potential and has been used to mitigate inflammation, modulate immune responses and promote tissues generation<sup>53</sup>.

In order to extract statistical features to describe texture characteristics of MSC images, a 1960's technique called Gray Level Co-occurrence matrix (GLCM) may be helpful.

## 1.6. Gray Level Co-occurrence matrix (GLCM)

For this work, it is important to extract MSC texture information from this image using the spatial relationship between pixel intensities. We used the Gray Level Co-occurrence Matrix (GLCM), a statistical method for this image processing<sup>6</sup>. We adopted the GLCM technique because it has a superior ability for tasks like texture classification for confluent cells. Others have used the GLCM for brain tumor classification<sup>92</sup>. Additionally, GLCM has been used for remote sensing, specifically for analyzing satellite imagery for land cover classification<sup>65</sup>. It has also been used for image classification to distinguish between different types of images based on their texture<sup>66</sup>. For image classification, the technique works by extracting the spatial relationship of pixel in the GLCM, then the statistical correlation, energy, and homogeneity are calculated for classification. Furthermore, meteorologists use GLCM method to gather information about convective clouds to help predict severe weather events like wind speed, hailstorms, or flooding<sup>68</sup>.

For my proposed work, GLCM is used to extract statistical features like contrast, correlation, energy, homogeneity, and dissimilarity that will describe the texture characteristics to describe my biological images. Also, these features can be used as inputs in machine learning algorithms to extract image classification. What follows explains how GLMC technique works.

The GLCM technique was developed by Robert Haralick in 1973 and calculates how frequently pairs of pixels appear at a certain distance and orientation in a given image. The technique examines how often p(i,j) different combinations of pixel intensities occur in a specified spatial relation or the probability value of the GLCM. The reference and neighbor intensity pair of (i,j) entries represent a pixel with intensity i adjacent to a pixel with intensity j. These assignments of (i,j) pixel intensities generate an intensity matrix corresponding to grey

levels within an image. In this case, i and j runs from 0, 1, 2, ..., N-1 within the  $N \times N$  matrix. The spatial distribution creates a map of textures to characterize the texture, capturing critical characteristics of the image that help in tasks like classification, segmentation, and other statistical measures. Some of the major features, with their corresponding equations, of the GLCM are contrast, dissimilarity, homogeneity, energy, entropy, and correlation are described below<sup>6,28</sup>. In all the associated equations of the features, the summation runs from  $0 \rightarrow N-1$ , since the first cell in the upper left of the GLMC is (i,j) = (0,0), i.e., the i value (0) of this cell is the same as the value of the reference pixel, j=0.

**Contrast:** The contrast measures the intensity difference between a pixel and its neighbor over the entire image using equation 1.

$$\sum_{i,j=0}^{N-1} p_{i,j}(i-j)^2 \dots \dots (1)$$

In this contrast equation, the term i-j is referred to as the weight. For i=j, (i-j)=0, meaning the cell is on the diagonal. These diagonal values represent pixels similar to their neighbors with a weight of 0. For i-j=1, means small contrast with a weight of 1. i-j=2, means increasing contrast with a weight of 4, and increases exponentially as i-j gets larger. Higher values indicate more variation in intensity, often meaning a rougher or more textured surfaces.

**Dissimilarity** – The dissimilarity feature is similar to contrast but gives a slightly different emphasis on the degree of variation between neighboring pixels using equation 2.

$$\sum_{i,j=0}^{N-1} p_{i,j} |i-j|^2 \dots \dots (2)$$

In this equation, the term i-j is the dissimilarity weight. For i = j, i - j = 0; i - j = 1, i - j =

**Homogeneity** – The homogeneity feature evaluates the closeness of the distribution of elements in the GLCM to the diagonal using equation 3.

$$\sum_{i,j=0}^{N-1} \frac{p_{i,j}}{(1+(i-j)^2)} \dots \dots (3)$$

In this homogeneity equation, the term  $\frac{1}{(1+(i-j)^2)}$  is the weight. Higher homogeneity means that similar intensity levels are closer together, indicating a smoother or more uniform texture. The homogeneity weights decrease exponentially away from the diagonal.

**Energy** – The energy feature represents the sum of squared elements in the GLCM, often seen as a measure of image uniformity using equation 4.

$$\sum_{i,j=0}^{N-1} (p_{i,j})^2 \dots \dots (4)$$

Higher energy value indicates more uniform textures with less variability<sup>8</sup>.

**Entropy** – The entropy feature measures the randomness or complexity in the image texture using equation 5.

$$\sum_{i,j=0}^{N-1} p_{i,j}(-Ln \, p_{i,j}) \dots \dots (5)$$

In equation 5, since Ln (0) is undefined, we assume 0 \* Ln 0 = 0.  $p_{i,j}$  is a probability so  $0 \le p_{i,j} \le 1$ , hence Ln  $p_{i,j}$ , is either 0 or negative. Higher entropy values mean more disorder or complexity, often found in highly textured or chaotic regions.

**Correlation (r)** – The correlation feature looks at the linear dependency between pixel intensities at specific positions relative to each other using equation 6.

$$r = \sum_{i,j=0}^{N-1} \frac{(i-\mu_i)(j-\mu_j)}{\sigma_i \sigma_j} \dots \dots (6)$$

In equation 6,  $\mu_i$  is the mean reference,  $\mu_j$  is the mean neighbor,  $\sigma_i$  is the standard deviation reference,  $\sigma_j$  is the standard deviation neighbor, and r is the correlation. These quantities are calculated using equations 7-10.

$$\mu_i = \sum_{i,j=0}^{N-1} i * p_{i,j} \dots \dots (7)$$

$$\mu_j = \sum_{i,j=0}^{N-1} j * p_{i,j} \dots \dots (8)$$

$$\sigma_i^2 = \sum_{i,j=0}^{N-1} p_{i,j} (i - \mu_i)^2 \dots (9)$$

$$\sigma_j^2 = \sum_{i,j=0}^{N-1} p_{i,j} (j - \mu_j)^2 \dots \dots (10)$$

Higher correlation values suggest pixel intensities are more predictable and aligned, indicating a structured or patterned texture<sup>8</sup>. Since the correlation calculation is quite different from the other texture measures, it gives different information and can thus be used in combination with another texture measure.

Although MSCs have great potential, there is still work that needs to be done to advance clinical trials. Using a combination of DPC imaging, GLCM methods, and the current gold standard of measuring osteogenic differentiation, it may be possible to determine or tell the quality of MSC differentiation potential earlier and also help bridge the gap between information among analysis methods. Alkaline Phosphate (ALP) activity assays are typically used to look at early-stage differentiation occurrence, Alizarin red staining usually is limited to late-stage differentiation as well as being a quantitative approximation. In the ideal scenario imaging can help support data from both these assays as well as being used with machine to determine day of differentiation of the cell early stages.

Due to the lack of a reliable non-destructive and inexpensive standard, this limits the ability to assess osteogenic differentiation potential earlier on. This work uses phase microscopy techniques to assess potency assays correlated with osteogenic differentiation outcomes in five

cell lines. Success implementation of this method can significantly reduce the time, money, and resources needed to identify viable donor cell lines.

## 1.7. ALP activity and Alizarin Red assay

Two commonly used osteogenic markers that used in MSC work are the alkaline phosphatase (ALP) activity and calcium deposition. In this work, in order to evaluate the osteogenic differentiation, ALP activity and Alizarin Red staining were used. ALP captures early-stage commitment during the osteogenic differentiation process, while Alizarin reflects later mineral deposition. Both assays are widely used to measure differentiation progress and were therefore included to cover the full differentiation timeline. One assay or both may be helpful when choosing an endpoint assay to compare with phase features.

### **CHAPTER 2:**

## **EXPERIMENTAL DESIGN AND METHODS**

## 2.1. Cell culture

The human cells used in this project were obtained from Rooster-Bio Inc. with product names RoosterVial<sup>TM</sup>-hBM-10M (part number MSC-001) and RoosterVial<sup>TM</sup>-hBM-1M-XF (part number MSC-031). All the cells were stored in liquid nitrogen (LN<sub>2</sub>). The specifications of these products, from four different hBM donors, are listed in Table 3.

Table 3: Specifications of cells used in this experiment.

	RoosterVial <sup>TM</sup>				
	-hBM-10M	-hBM-10M	-hBM-10M	-hBM-1M-XF	-hBM-
	(RB175)	(RB177)	(RB183)	(RB277)	(RB071)
Tissue Origin	Human bone				
	marrow	marrow	marrow	marrow	marrow
Donor Age	25	22	26	29	20
Donor Sex	Male	Male	Female	Male	Female
Population	8.8	8.2	8.9	Not available	8.9
Doubling					
Level					
Date of	01.26.2017	02.01.2017	02.06.2017	01.30.2020	08.18.2017
Manufacture					
Date of	01.26.2019	02.01.2019	02.06.2019	01.30.2024	Not available
Expiration					

Cells were collected from the liquid nitrogen tank and cultured in a T-175 flask for 3-4 days. Cells were cultured under standard conditions of 37°C and 5% CO<sub>2</sub>. After the 3-4 days period, the cells were then seeded at a density of 10,000 cells/cm<sup>2</sup> with MEM-α medium in four

separate 24 well plates (microplates). Each of the four 24-well plate was assigned a day name, based on the day the cells are intended to be harvested. The assigned day names were Day 7 plate, Day 14 plate, Day 21 plate and day 28 plate respectively as shown in table 4. In these labeling, microplates set 1 are designated for cells to be analyzed on Day 7, microplates set 2 are designed for the cells to be analyzed on day 14, and so on. The four 24-well plates translated to 96 individual wells.

Table 4: Labeling of the four 24 well plates (Microplates)

Microplates set 1	Microplates set 2	Microplates set 3	Microplates set 4
Day 7 analysis plate	Day 14 analysis plate	Day 21 analysis plate	Day 28 analysis plate

After cells grew to confluence 1-2 days, the MEM  $\alpha$  medium was changed to homemade OIM. The preparation of the OIM was done using this formula below

a. 
$$desired\ amount\ of\ OIM\ (mL)\ 250*\frac{10mMoles}{1L}*\frac{216.04g}{1\ mole}*\frac{1\ mole}{1000\ milimoles}*$$

$$\frac{1L}{1000\ mL}=amount\ (g)=.540\ grams$$

The desired amount of  $\beta$ -glycerophosphate was calculated based on the final volume of OIM needed (e.g., 250 mL requires 0.540 grams). After the addition of the media to a 250mL container, 40mL of this media was used to dissolve the  $\beta$ -glycerophosphate in a separate conical tube and then put into a water bath. Dexamethasone from a .01M stock solution was added to the remaining OIM at a rate of  $1 \mu L$  per 30 mL of OIM (e.g., 2.5  $\mu L$  for 250 mL).

,Sequestered 40 mL media was used to dissolve the β-glycerophosphate in a water bath. Dexamethasone was then added from a 0.01 M stock solution at a rate of 1  $\mu$ L per 30 mL of OIM (e.g., 2.5  $\mu$ L for 250 mL). L-ascorbic acid was then added at 1  $\mu$ L per mL of total media (e.g., 250  $\mu$ L for 250 mL OIM). The conical tube with the now dissolved β-glycerophosphate from the water bath was gently added to the media with the previously mentioned ratios.

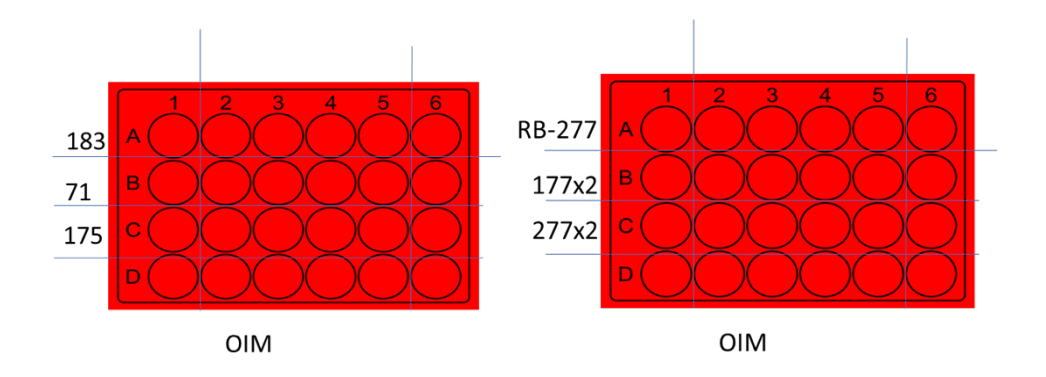
The OIM was changed every 1-2 days for the 24 well plates throughout the experiment period. The cells were counted using the BIO RAD, TC20 Automated Cell Counter.

### 2.2. Image Collection

A Differential Phase Contrast (DPC) microscope was used to collect cell images. First, the cell samples were carefully prepared on a slide. To achieve high-quality image results, the DPC optics were set up for maximum focus. The exposure time was 400-ms and the objective lens at 10x. The illumination source was then aligned and with the DPC set to automated mode, multiple individual images were captured at four different illumination angles for each well. The imaging process, at the four different illumination angles, was used to complete half of the 24-well plates. These multiple individual images were then stitched together using Fiji software (an open-source image analysis tool) to create a montage to offer better lateral resolution. The stitching of the individual images was done for every well with the exception of the first and last columns (Columns 1 and 6) of wells due to microscope limitations.

The DPC microscope was used to obtain a more detailed view of the cell features and components, that was difficult to observe using the brightfield microscope. Additionally, the

DPC was effective at visualizing the transparent and colorless specimens, able to enhance the contrast of the boundary between cellular membranes to produce high-contrast images and produced a greater depth of field.



## 2.3. Alizarin Red staining and quantification

After the differentiation period for the various timepoints, MSCs were washed twice with phosphate-buffered saline (PBS) to remove residual media. MSCs were then fixed with 4% paraformaldehyde for 15 minutes at room temperature and washed again with PBS. Alizarin red stain was made and used in each of the wells that were used for imaging. MSCs were incubated with a 2% alizarin red S solution (pH 4.2) for 25-30 minutes at room temperature, with gentle rocking. Wells were then imaged using a brightfield microscope camera at 7-9 different locations. The brightfield microscope camera (Hongxiangs, Zeiss Axio Vert.A1 MET Brightfield) was used to capture images of the cells. These images were collected and quantified using a custom code to calculate the number of red pixels in an image. The Alizarin red is an anthraquinone derivative, binds to calcium ions, forming a bright red complex.

## 2.4. ALP Activity Assay

Alkaline Phosphate (ALP) activity was assessed after the various time points Day 7, Day 14, Day 21 and Day 28 for the MSCs used. The MSCs were rinsed using PBS, pealed up into a conical tube and lysed using a Dounce homogenizer. The lysates were then centrifuged at 13,000 x g for 15 minutes at 4°C, and supernatants were collected for the ALP assay. An ALP activity kit (calorimetric assay) was used and in accordance to measure the total protein content. The colorimetric assays detected the enzyme's activity by measuring the hydrolysis of a phosphate substrate, p-nitrophenyl phosphate (pNPP), which releases a yellow product. Incubating MSC lysates with p-nitrophenyl phosphate (pNPP) substrate. The reaction was stopped using stopping solution provided, and the absorbance was measured at 405 nm using the microplate (SpectraMaxiD5) reader in the lab building. Two of the wells used for imaging from the 24 well plate were put in the 96-well plate as a triplicate. A standard was used from the ALP activity kit to calculate the ALP using the absorbance.

### 2.5. GLCM evaluation

The feature extraction from the images was done using a GLCM quantification code to break down the features into Contrast, Dissimilarity, Energy, Correlation and Homogeneity in accordance with equations 1 through 10 from sections 1.5. Spliced images were used to create the montage for the original images from the Differential Phase contrast microscope. The next section shows the results of (i) Differentiation of MSCs using gold standard of Alizarin Red Staining and ALP Activity Assays, (ii) ALP vs. percent differentiated images, (iii) Differential phase contrast images, and (iv) GLCM figures. The GLCM was used to analyze the texture of our cell images by examining the spatial relationships between pixels. The GLCM allowed us to

identify featured like cell morphology, nuclear texture, and presence of certain cellular components.

## 2.6. Statistical Method

In this work, we hypothesize that morphological changes that occur in the MSCs during their differentiation process can be monitored and assessed through phase microscopy techniques. To validate our hypothesis, we plan to use p-statistics. Specifically, p-values of regression lines generated from experimental data would be used to measure the probability of obtaining the observed results. The p-values are a measure of the probability of seeing the observed difference. The visual short-hand to indicate the level of significance associated with p-value were adopted for interpreting the likelihood that the observed difference is genuine if the null hypothesis is true.

Table 5: p-value interpretations.

p-value	interpretation
p ≤ 0.05 *	Significant
p ≤ 0.01 **	Very significant
p ≤ 0.001 ***	Highly significant
p ≤ 0.0001 ****	Extremely significant
p > 0.05 NS	Not significant

## **CHAPTER 3:**

## **RESULTS**

# 3.1 <u>Differentiation of MSCs using of Alizarin Red Staining and ALP Activity Assays</u>

# 3.1. Alizarin Red Staining

Figure 3.1.1 shows the brightfield representative images for the MSC donors RB183, RB71, RB175, RB177, and RB277 (as referred in table 3) from left to right at Day, 7, Day 14, Day 21, and Day 28. About 7-9 images were taken per well and the representative images of the time points for their respective donors can be observed below.

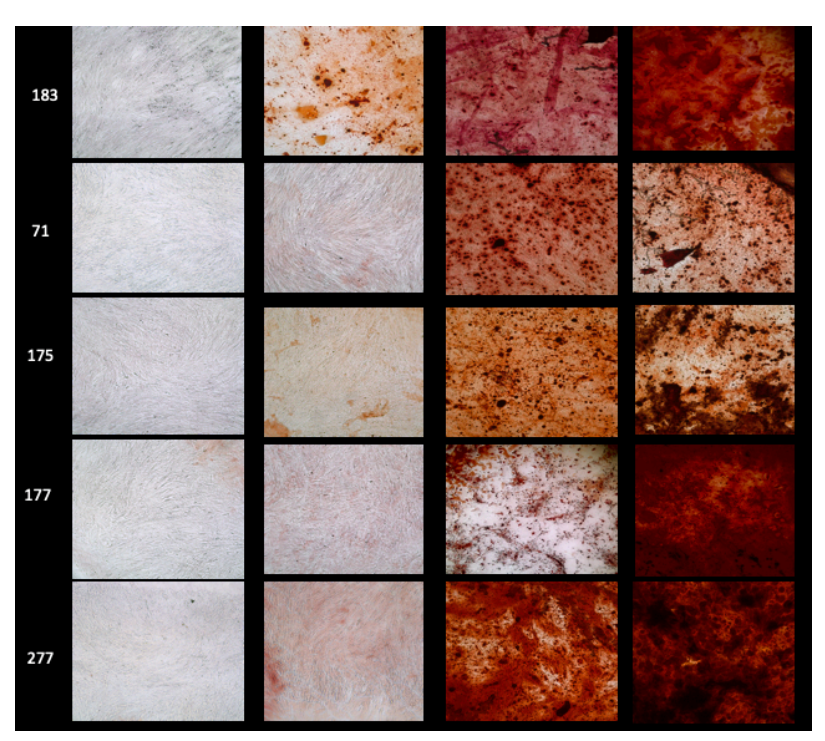


Figure 3.1.1: Comparison of the Alizarin red staining over 28 days for the five cell lines (RB183, RB71, RB175, RB177, and RB277).

The intensity of red increases as the cells differentiates over time corresponding to level of mineralization. Figures 3.1.2 shows the Alizarin red trend lines for RB175, RB177, RB183, RB277, and RB71. For Figure 3.1.2, the red staining accumulation over time was captured using the red pixel count across days 7, 14, 21, and 28 for each cell line. The red staining correlates to the amount of calcium deposits left by the cells.

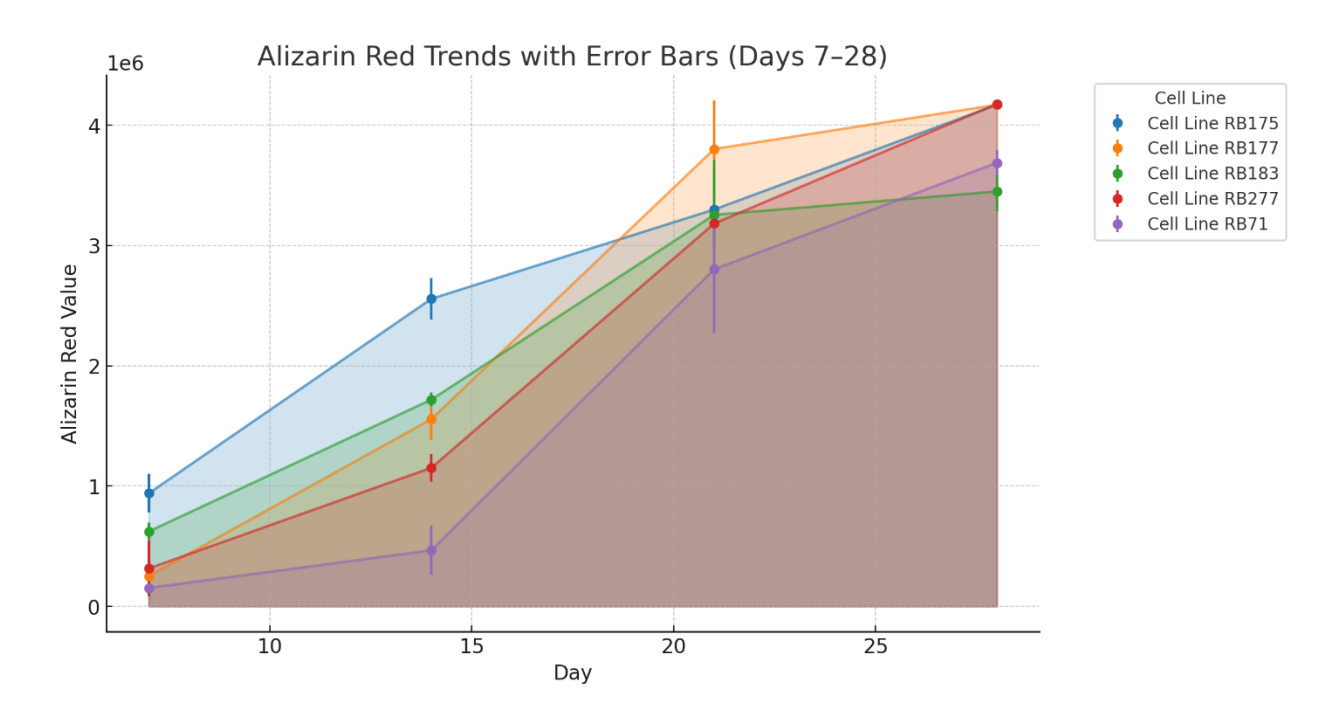


Figure 3.1.2: Alizarin Red Trends for all five cell lines from day 7 through day 28.

To dynamically measure and analyze the differentiation of each cell line across the days, the AUC) of Figure 3.1.2 was calculated to generate figure 3.1.3. Figure 3.1.3 shows a bar graph of the corresponding area under the curve (AUC) for each of the cell lines.

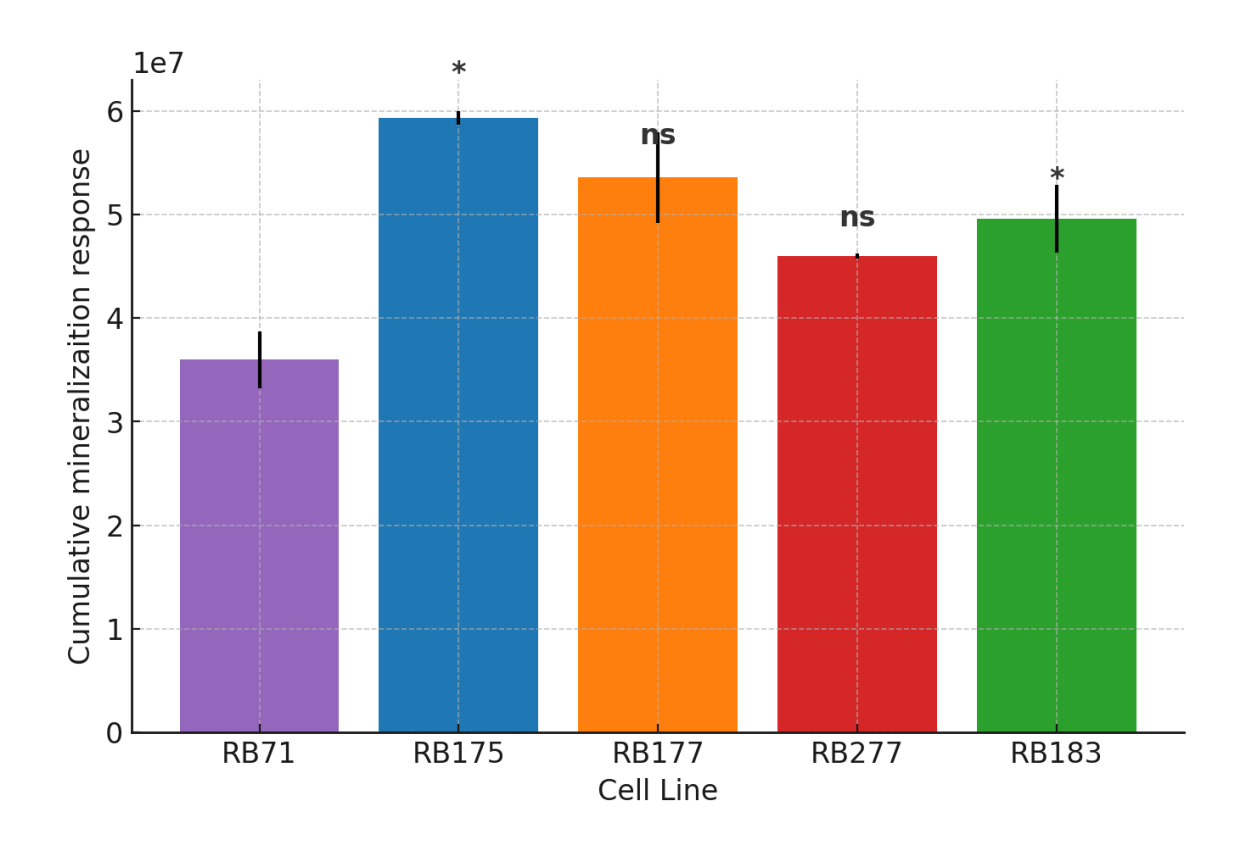


Figure 3.1.3: Area under the curve (AUC) for RB71, RB175, RB177, RB277, and RB183 from day 7 through day 28.

Another assay that was used was the ALP activity assay to help decide which method would be best to use as an endpoint assay. The ALP activity method is a common early detection test of osteogenic differentiation. Below we show our ALP activity results across the four time points.

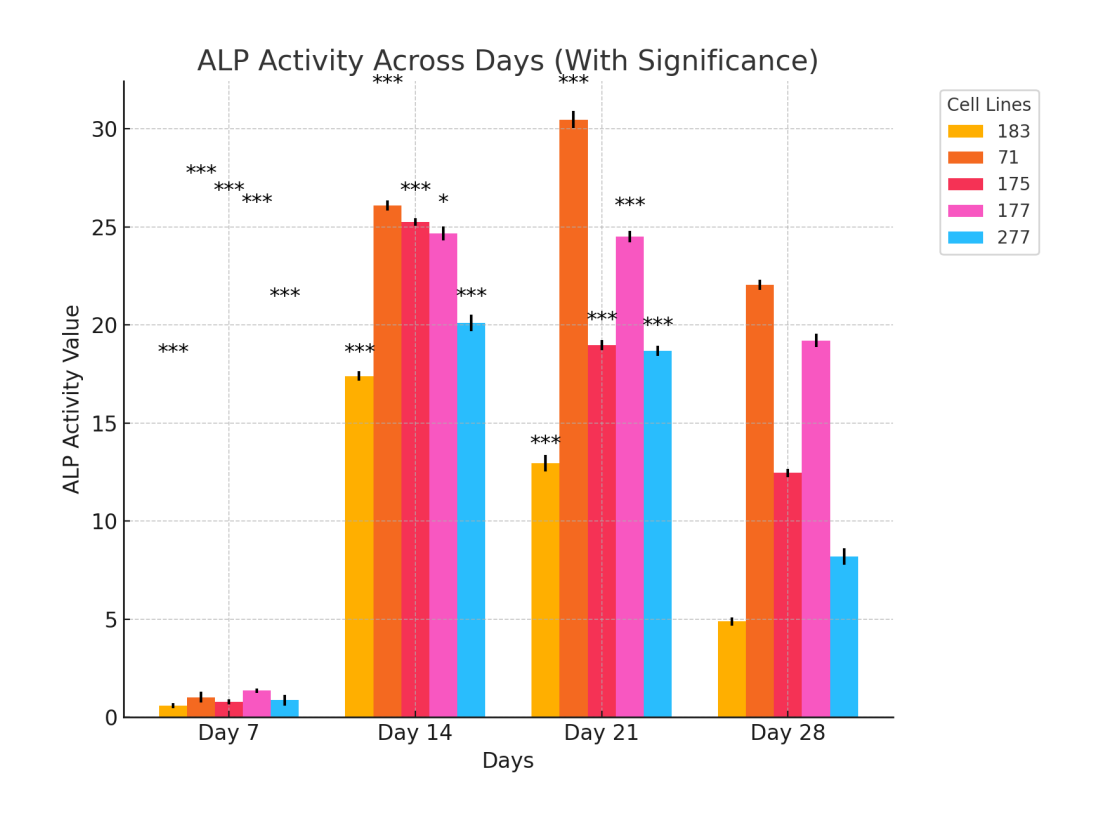


Figure 3.2.1: ALP Activity for cell lines for RB183, RB71, RB175, RB177, and RB277 across Days

The ALP was measured using the hydrolysis of a phosphate substrate, p-nitrophenyl phosphate (pNPP), which releases a yellow product. The yellow product was compared to a standard from a standard from the ALP activity kit. From our results, we noticed more ALP activity detection in days 14 and day 21 across all cell lines than activity levels in days 7 and day 28.

Next phase microscopy was used to take half-well images of the cells at different time points to examine the features of the cell lines. In particular, the differential phase contrast (DPC) was adopted.

# 3.3. Differential Phase Contrast Imaging over the differentiation process

Below are the half well images from the DPC microscope that were montaged together using Fiji to offer better lateral resolution. The grayscale images of the donors (RB183, RB177, RB277, RB71, and RB175) at the various time points are shown in figures 3.2.1, below

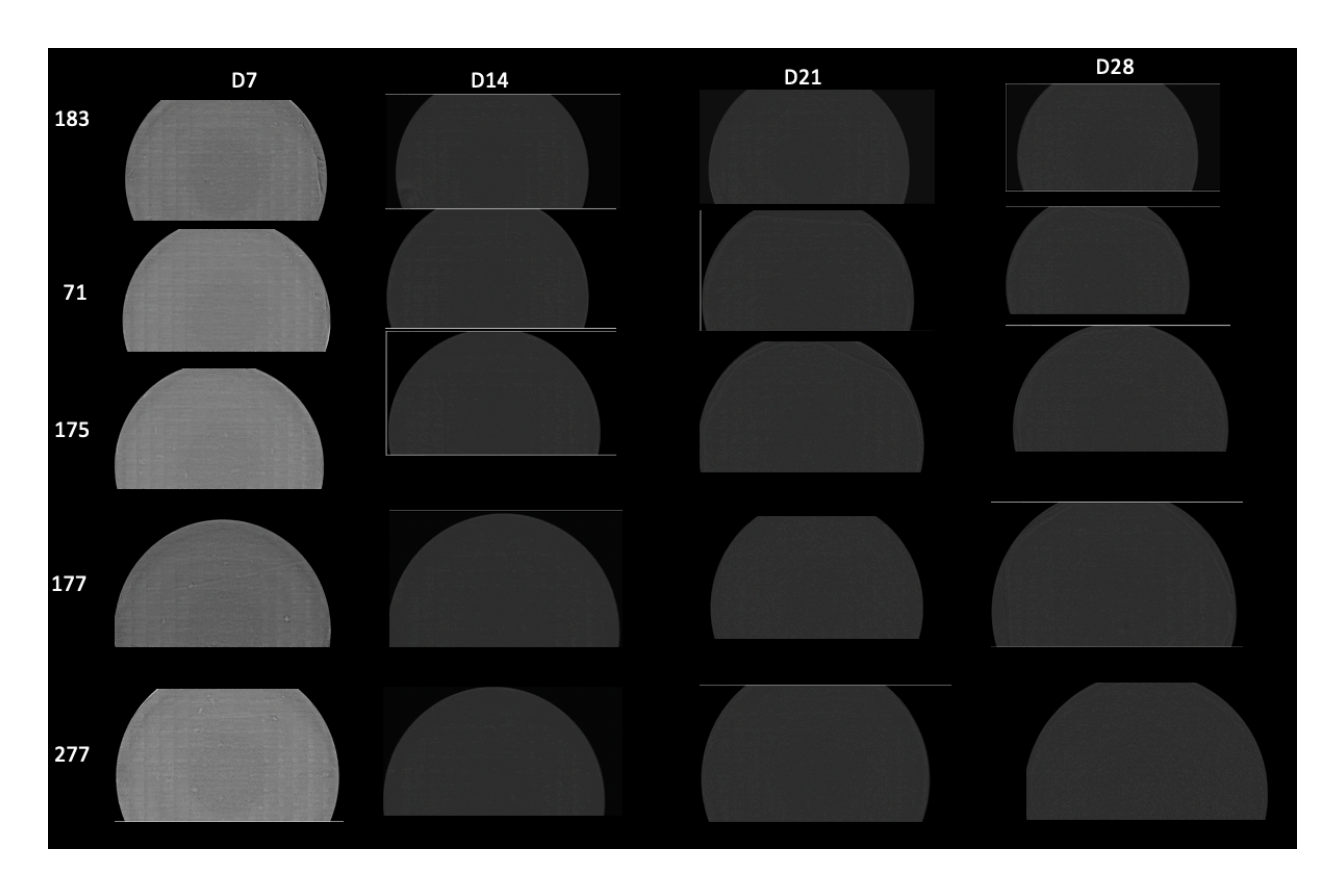


Figure 3.3.1: Normalized gray scale DPC images over 28 days for the MSC donors (RB183, RB177, RB277, RB71, and RB175).

DPC images were taken for RB183, RB177, RB277, RB71, and RB175 cell lines over 28-day period. For ease of viewing, a larger representative image at day 7 as well as day 28 are displayed in Figure 3.3.2 and Figure 3.3.3 for RB183. The aim here is to show the difference

from early day differentiation compared to late day and how much material the cells secret over time.

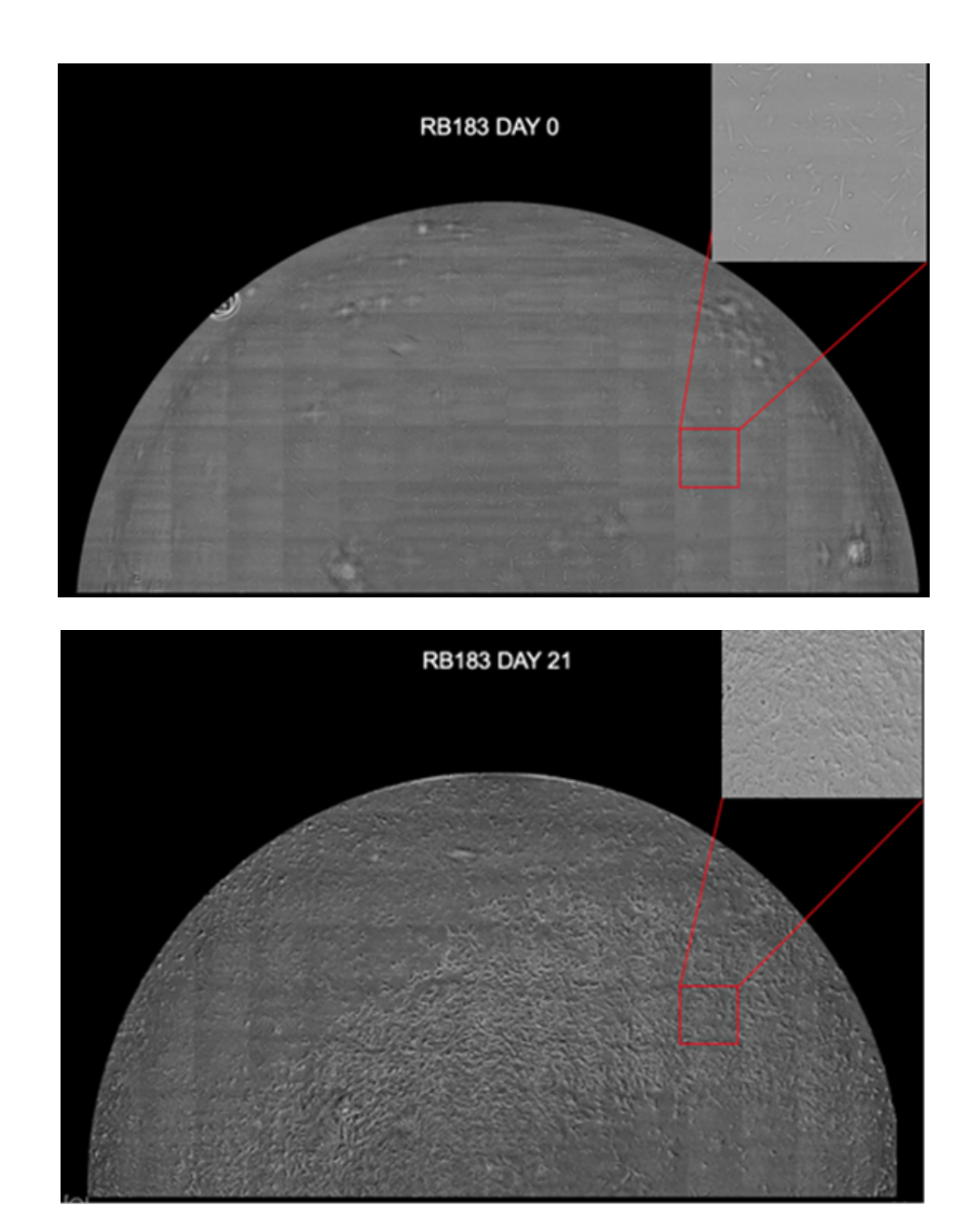
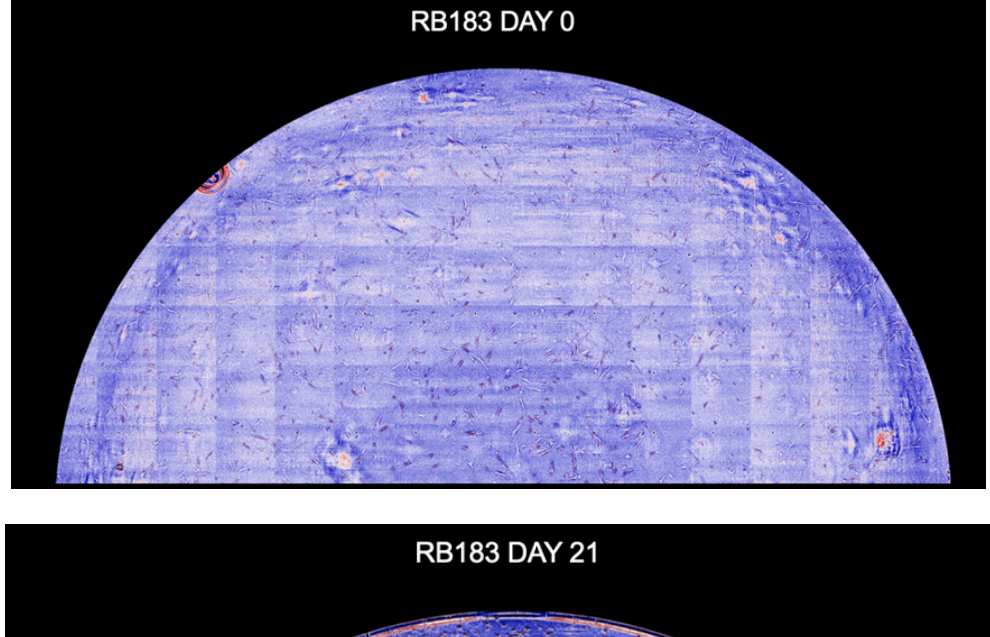


Figure 3.3.2: Grayscale images of RB183 on Day 7 vs Day 28. with a small zoomed in section of the 24 well plate

This image shows the progression of mineral deposits and extra cellular matrix from Day 7 to Day 28. This grayscale image is a representative image showing deposition as MSCs differentiate.



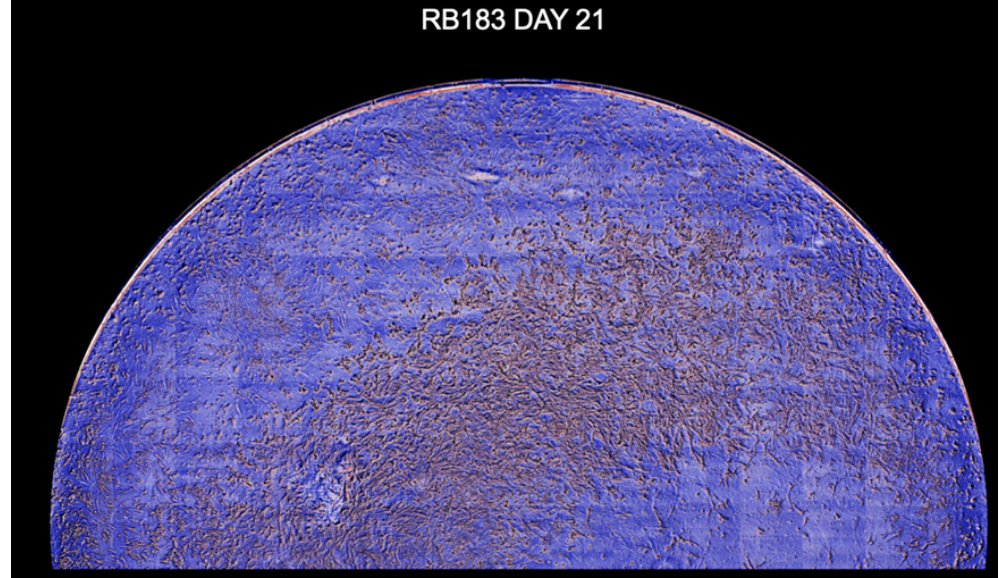


Figure 3.3.3: RB183 Day 7 vs Day 28 shows the progression of mineral deposits and extra cellular matrix from Day 7 to Day 28.

The images are the same as above however a look up table was applied to further show the mineralization. This mineralization can be seen in red on the Day 28 image. To extract

information from the phase images, we used the mean intensity over time across all cell lines. The information extracted are displayed in the section 3.4.

# 3.4. Mean intensity across days for all cell lines

Figures 3.4.1 shows the mean intensity line over time with the biological replicates. Each well for the biological replicates had 55 sub-images with their respective mean intensity values.

These intensity values were averaged to obtain the mean intensity per well per cell line per day.

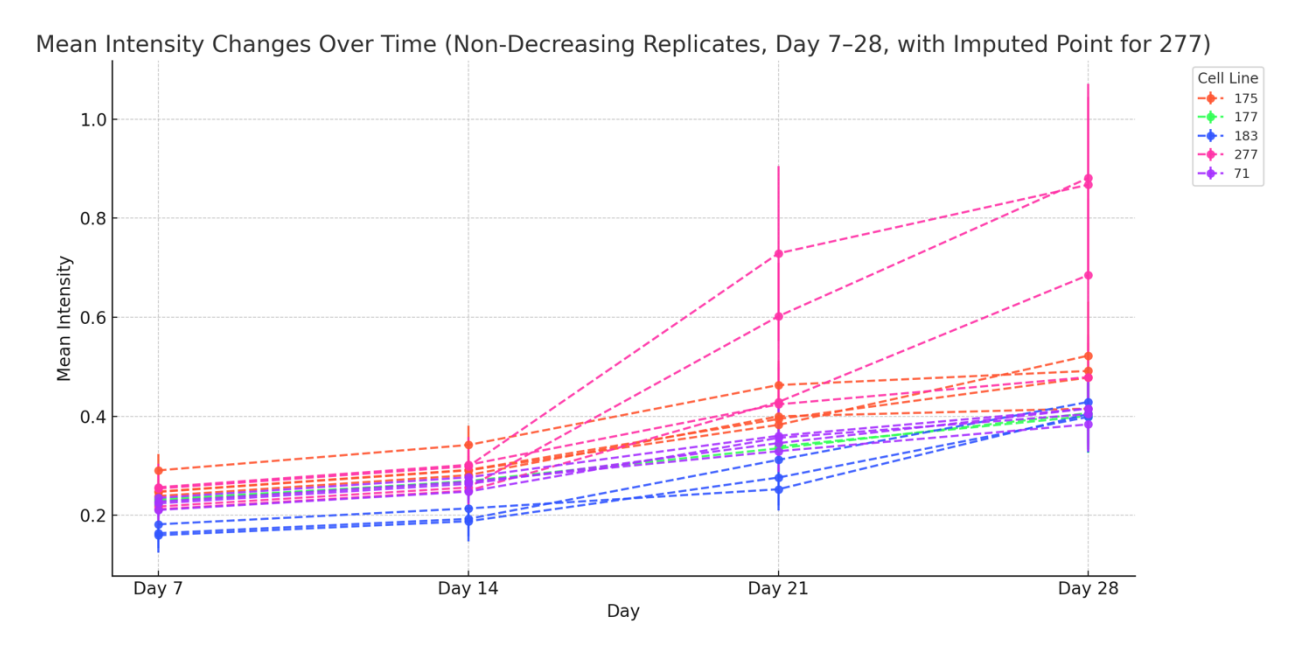


Figure 3.4.1: Biological replicates line graphs over time for the various cell lines across day 7, 14, 21, and 28.

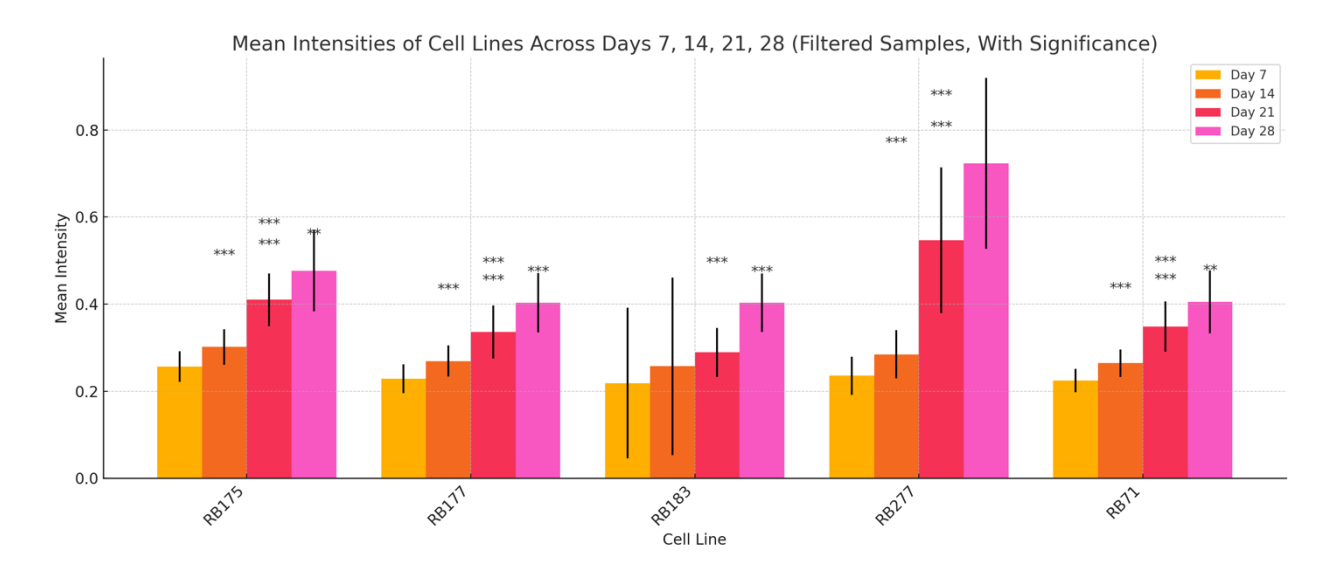


Figure 3.4.2: Mean Intensity bar graphs for RB175, RB177, RB183, RB277, and RB71 across days 7, 14, 21, and 28.

This bar graphs are the average mean intensity for each cell line with their respective biological replicates for various cell lines across Day 7, 14, 21, and 28. A p-test was done to determine the statistical significance between days for each cell line.

To quantify the image features during osteogenic differentiation, we used the gray level co-occurrence matrix (GLCM) to accomplish this task. Figure 3.5. below show the GLCM results.

# 3.5 Gray-level co-occurrence matrix (GLCM)

Each of the 55 sub images (per half-well), described in the earlier section, had their own GLCM values. Features involving the Contrast, Differentiation, Homogeneity, Dissimilarity and Energy were collected. These characteristics were compared over a 28-day period for the various donors (cell lines). A visualization of the sample spliced images of the montaged timepoints are shown below with a clear increase in mineralization over a 28-day period.

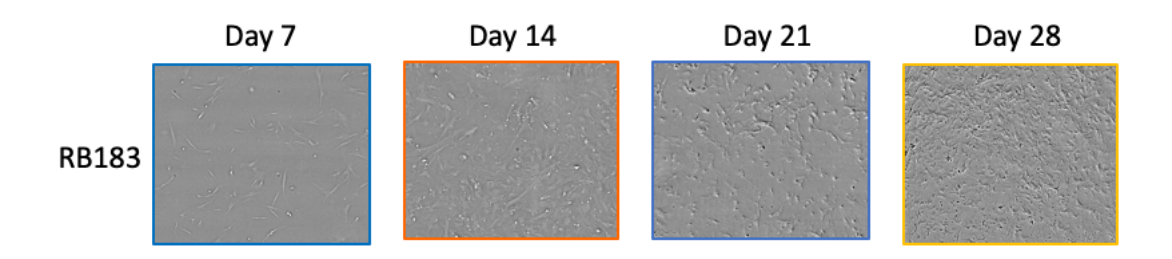


Figure 3.5.1: A visualization of the sample spliced images of the montaged timepoints are shown below with a clear increase in mineralization over a 28-day period.

In addition to the visualization of the sample spliced images, plots were taken for GLCM features (homogeneity, correlation, contrast, energy, and dissimilarity) versus offset range 0 –32. The figures 3.52 - 3.5.6 show GLCM features for RB183 cell line only over the 28-day period (Day7, Day14, Day 21, and Day 28) for MSC.

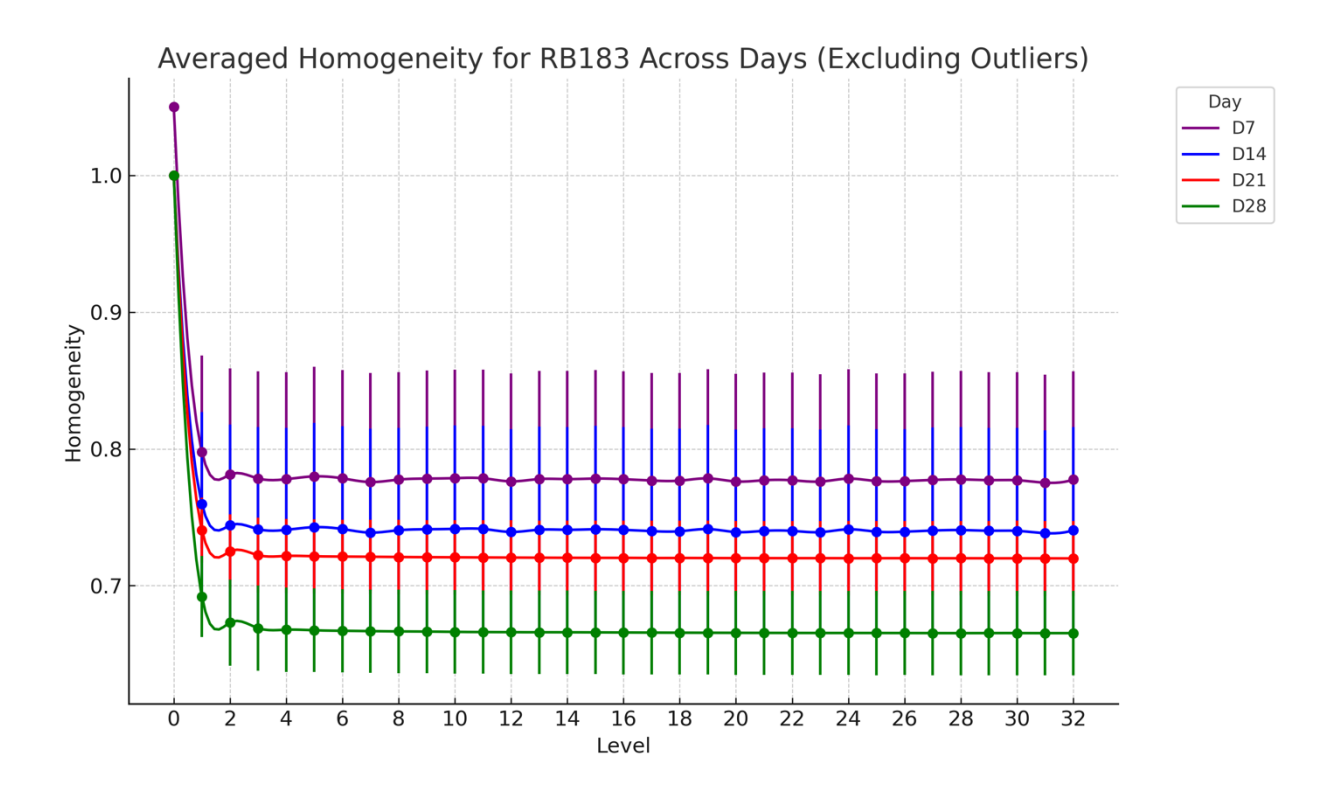


Figure 3.5.2: The averaged homogeneity for RB183 over 28 days shows a gradual decrease over time.

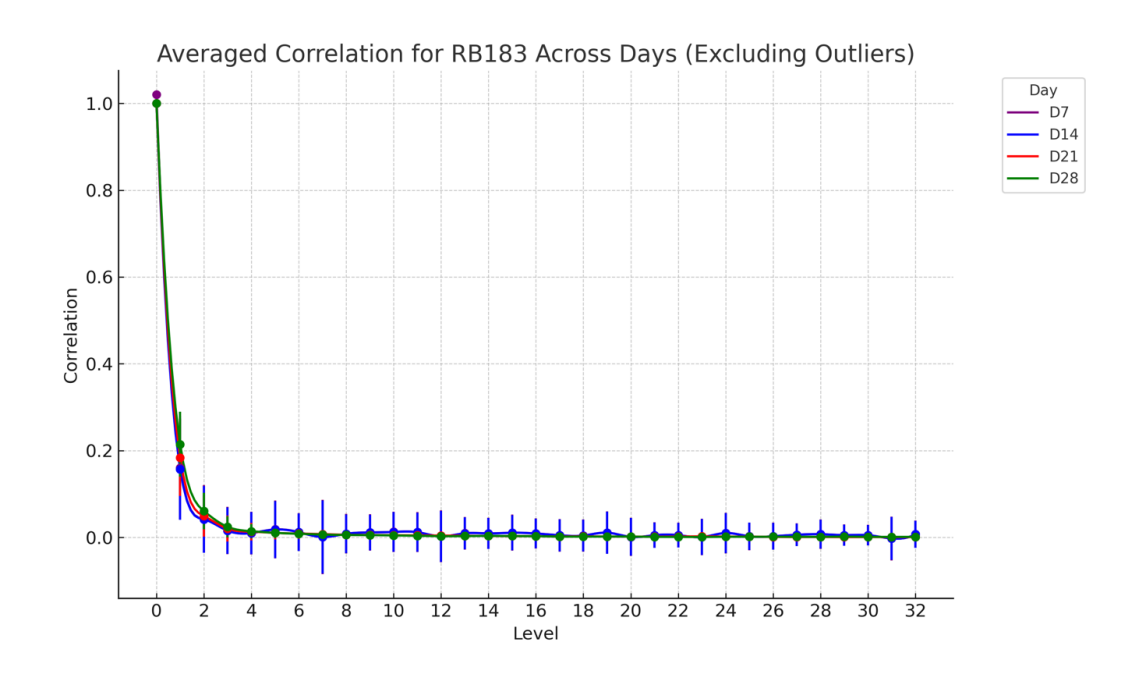


Figure 3.5.3: The correlation of the image shows a quick decrease to steady state over 28 days with no clear difference between the days.



Figure 3.5.4: The averaged contrast for RB183 over 28 days; the various time points differ with Day 28 having the highest contrast and day 7 having the lowest initial contrast.

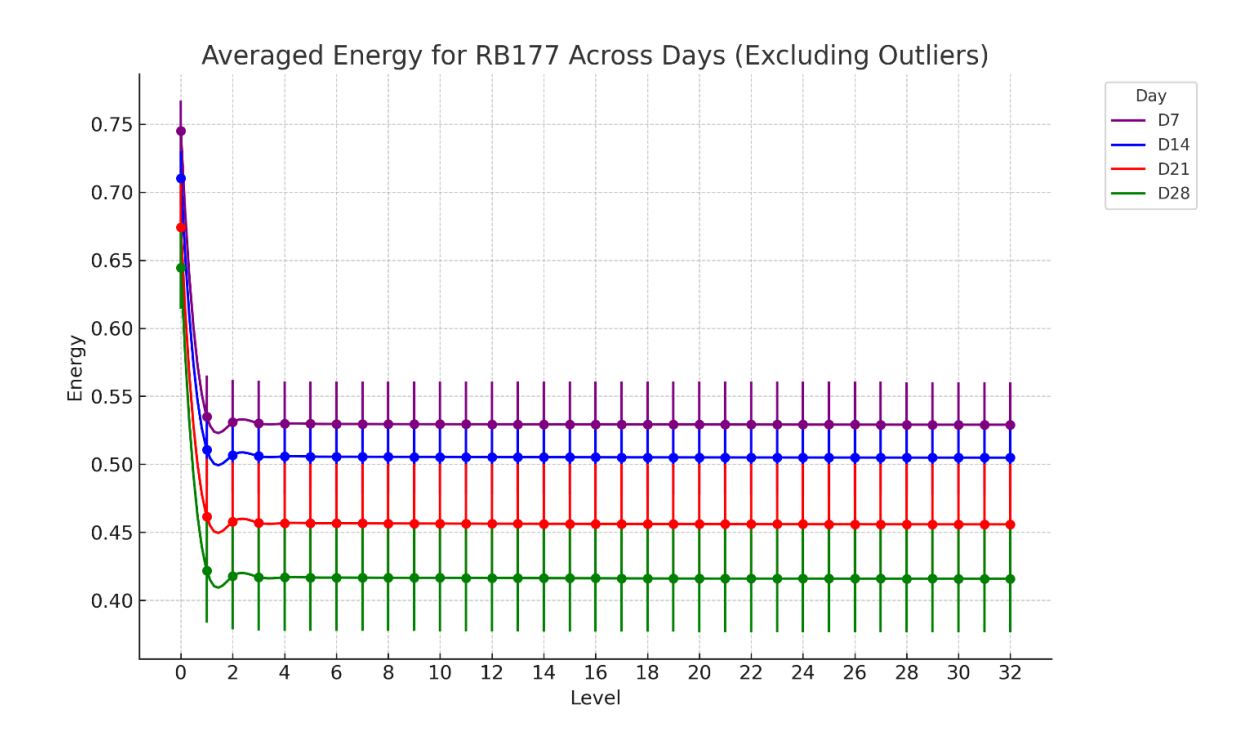


Figure 3.5.5: The averaged energy for RB183 over 28 days; donor at day 7 is highest with a steady decline to day 28 days of differentiation.

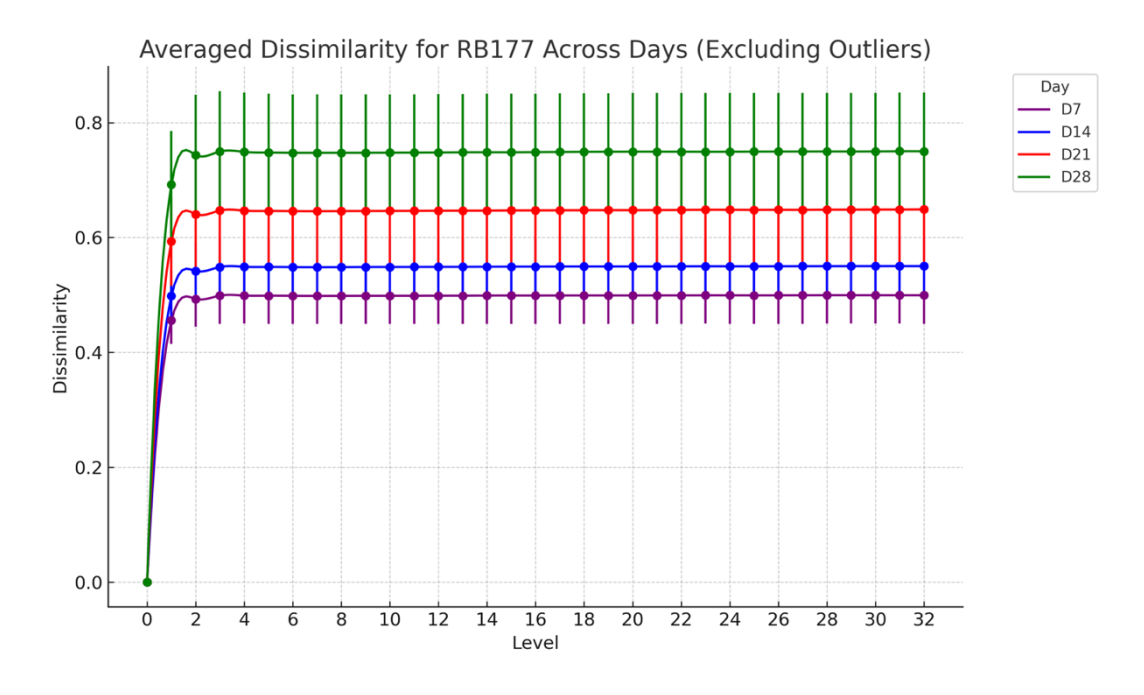


Figure 3.5.6: The averaged dissimilarity for RB183 over 28 days; differentiation is highest around day 28 and lowest around day 7 for the donor.

Similar GLCM analysis was done separately for the remaining 4 cell lines (RB175, RB177, RB277, and RB71). To better visualize the GLCM data generated, a Uniform Manifold Approximation and Projection (UMAP) space was used.

## 3.6. Visualization of GLCM features using UMAP space

A Uniform Manifold Approximation and Projection (UMAP) space was generated to create a multivariate comparison across the days based on all the GLCM features above. It is a non-linear dimensionality reduction technique. The UMAP was used to identify clusters and trends between the features for the cell lines at each day. This was done for all cell lines donors of MSCs. First the combined UMAP dimension reduction space was generated for all the cell lines as shown in the left standalone image. Next, the map was filtered out for each individual cell line to distinctly display the GLCM features described in the previous section.

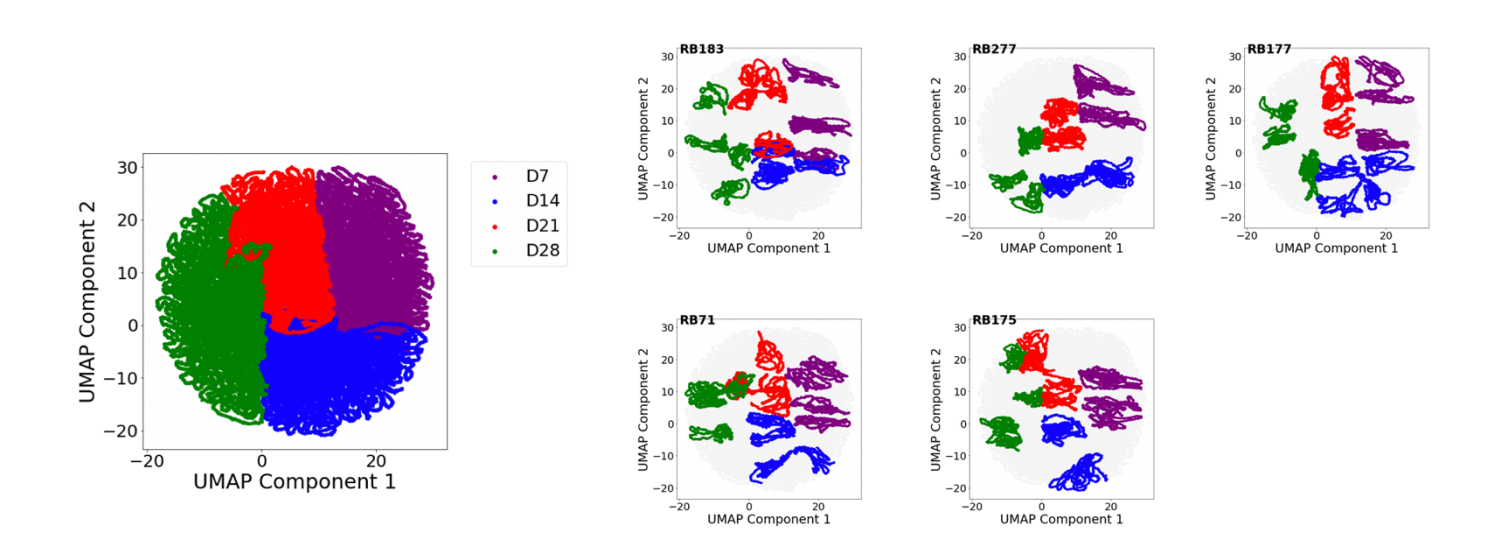


Figure 3.6.1: Combined UMAP dimensionality reduction filtered for all cell lines (RB175, RB177, RB183, RB277, and RB71).

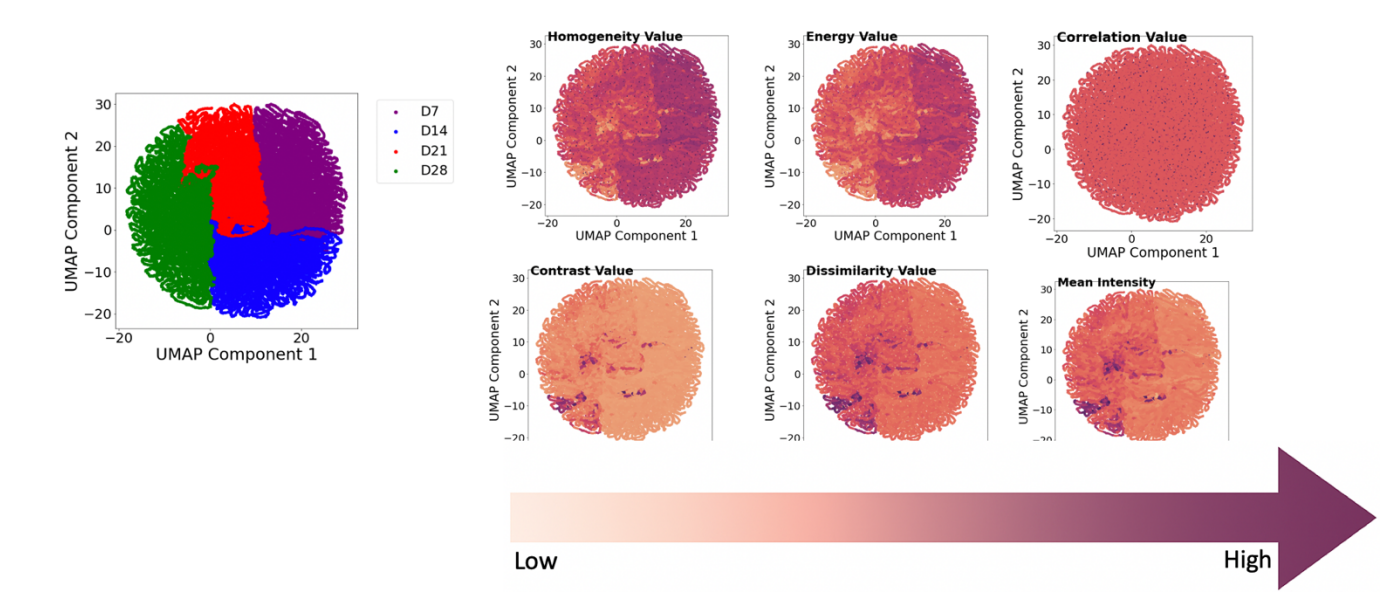


Figure 3.6.2: Showing a UMAP visual representation of trendlines seen in the GLCM graphs in the previous section for each of the GLCM features.

After using the UMAP to verify to GLCM features, we want to establish correlation between phase imaging features and Alizarin red staining.

## 3.7. Phase as a measure of differentiation progress

The following figure shows the correlation of the average phase features and the alizarin red. This was done with a random forest regression. The feature importance of what drives this regression model is shown on the right of the graph. The forest regression line shows the corresponding predicted mineral quantity versus actual day 28 Alizarin red for the different days. he best fit line across all days and the R<sup>2</sup> value of 0.974. The data captured in these figures shows the phase measure of the differentiation progress.

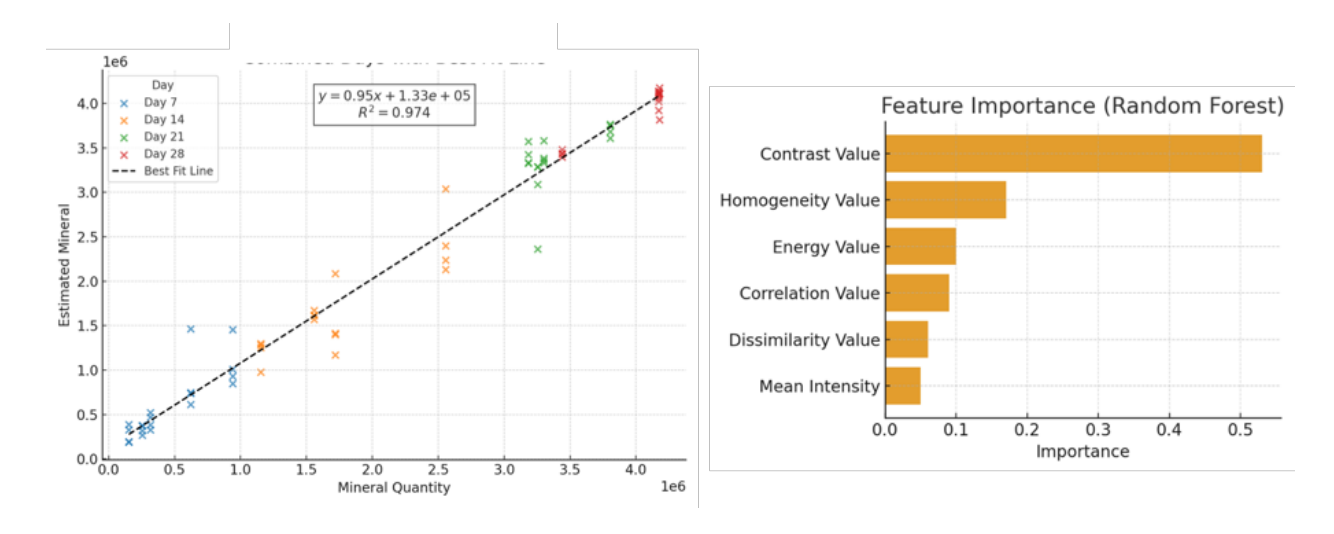


Figure 3.7.1 Shows the correlation between the phase features as well as Alizarin red value for each day for all cell lines.

# 3.8. Phase imaging to predict early detection differentiation potential

The next section shows the area under the curve (AUC) of the Alizarin red data curves for the phase imaging to predict early detection differentiation potential for the various days. The AUC was correlated to phase features of each individual cell line to see how strong the predictive model was and how strong it would be during earlier days.

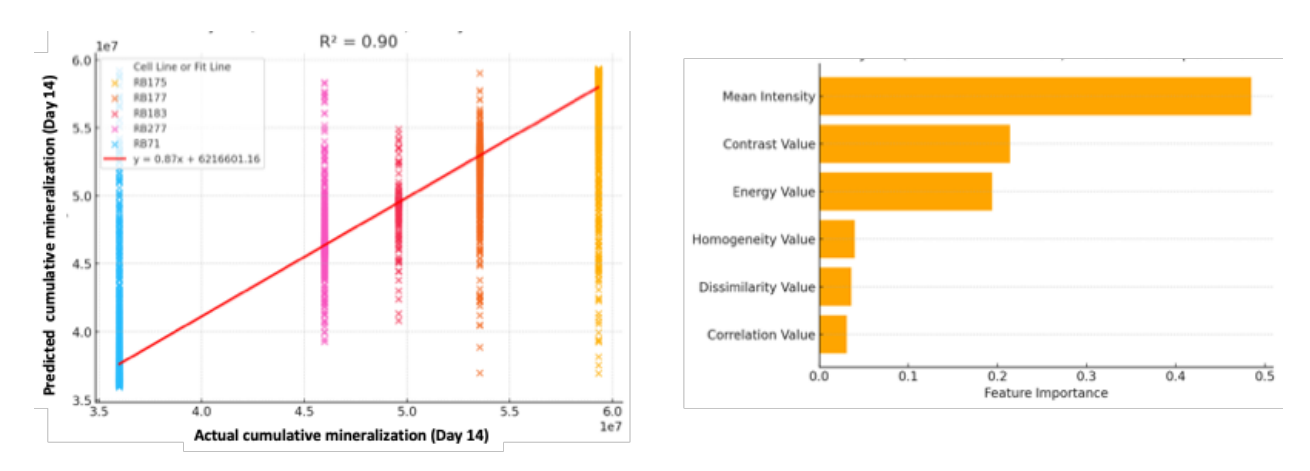


Figure 3.8.1: Random Forest Regression and feature Importance driving the regression line for Day 28 AUC (Day 7).

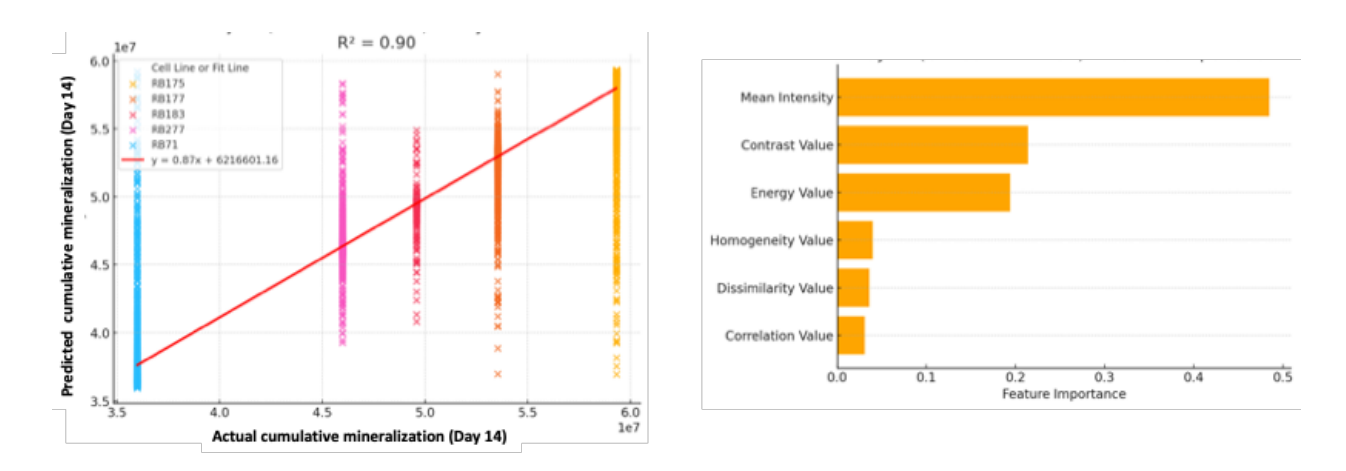


Figure 3.8.2: Random Forest Regression and feature Importance driving the regression line for Day 28 AUC (Day 14).

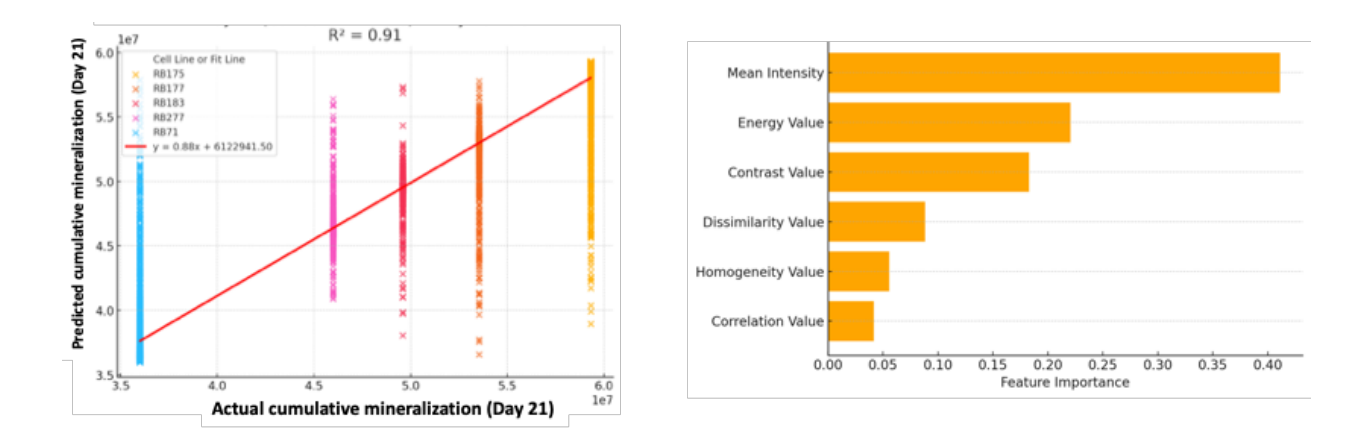


Figure 3.8.3: Random Forest Regression and feature Importance driving the regression line for Day 28 AUC (Day 21).

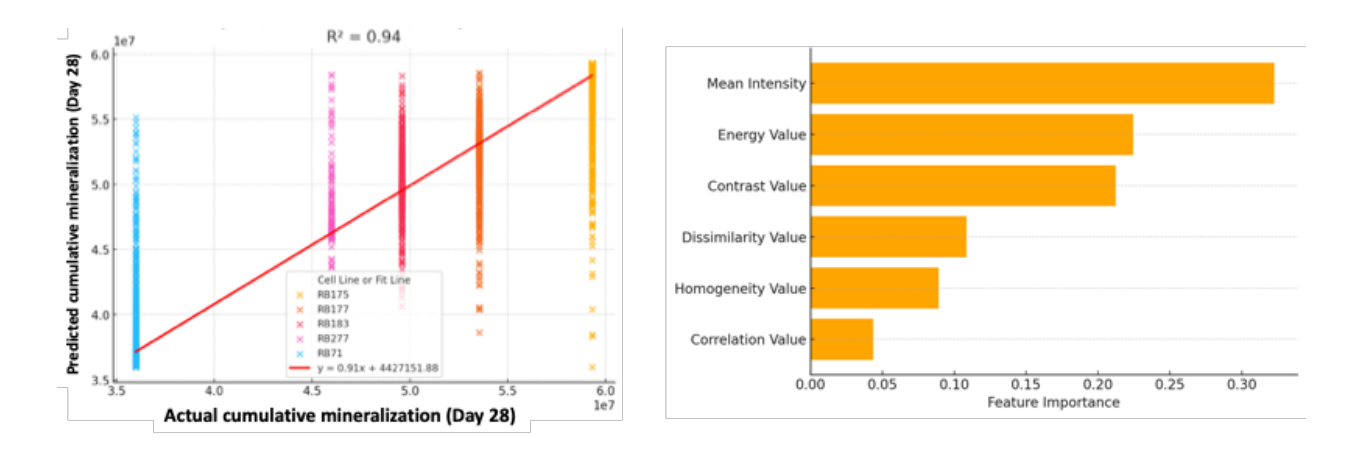


Figure 3.8.4: Random Forest Regression and feature Importance driving the regression line for Day 28 AUC (Day 28).

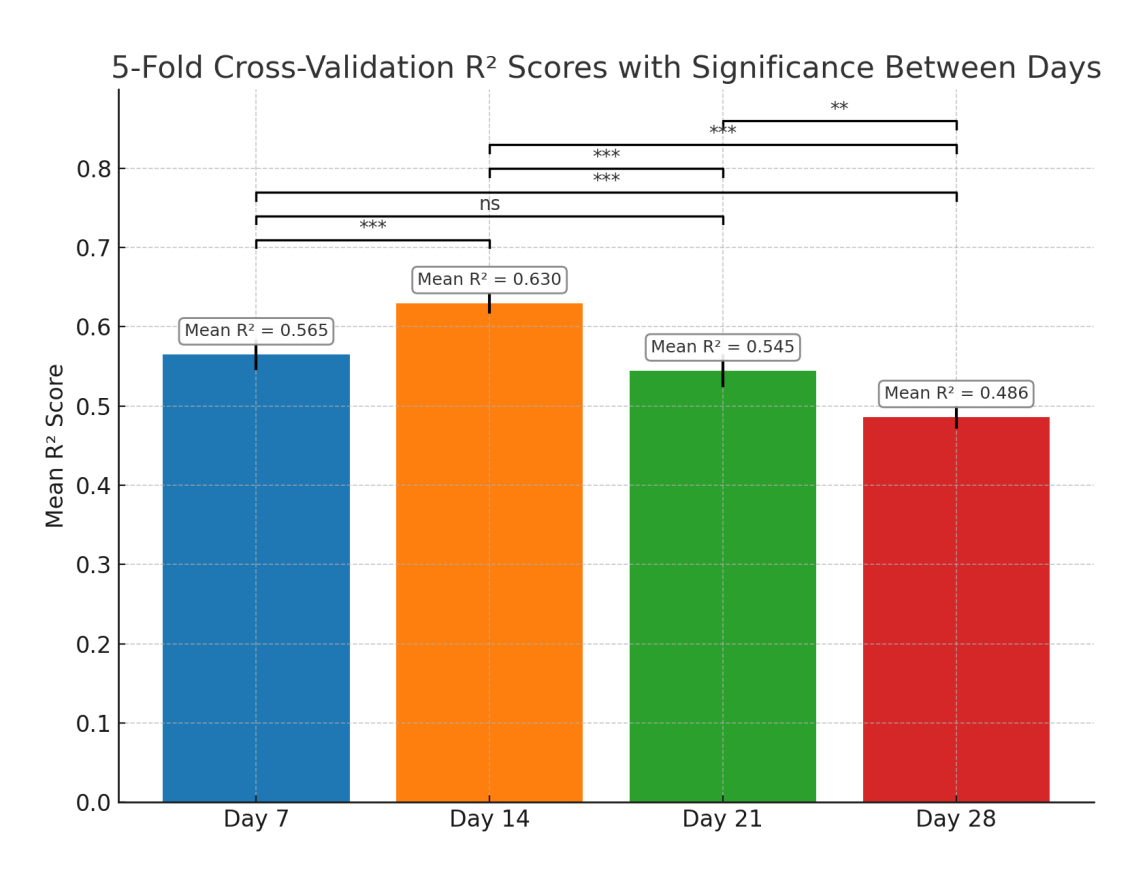


Figure 3.8.5: 5-fold cross validation R<sup>2</sup> scores with significance between days

To evaluate the overall performance of our machine learning, a 5-fold validation test was adopted. Figure 3.8.5 shows the performance results over the 28-day period.

### **CHAPTER 4:**

#### **DISCUSSION**

This work aims to address the lack of a non-destructive, scalable standard for assessing the osteogenic potential of MSCs by using phase imaging and machine learning to predict differentiation outcomes. Specifically, the goal is to quantify features from phase contrast images and evaluate their relationship to endpoint assays like ALP activity and Alizarin Red staining. This supports a broader need highlighted by the FDA to "demonstrate the relationship of potency measurements to the product's biologic activity," particularly in the context of developing meaningful, predictive potency assays for MSC-based therapies<sup>92</sup>.

#### 4.1. Alizarin red and ALP

Our Alizarin red results show that there are calcium deposits being a direct result of osteogenic differentiation. The ALP activity assay spiked early by day 14 and decreased by day 21 and 28 suggesting the role is more aligned with early osteogenic differentiation. The decline is consistent with literature results of ALP activity over a similar period. The ALP activity and Alizarin red staining results in this work shows that using Alizarin red as an endpoint measure was better for showing how far differentiation progressed by day 28. As such we used the Alizarin red as the end point measure for this work. Our results are consistent with literature with a steady increase in activity until around day 14 or 5 and a decrease at day 21 onwards. Similar trends were observed in a study that looked at the effect of Bio-Conditioning of Titanium

Implants for Enhancing Osteogenic Activity<sup>90</sup> and another that reported the visualization of Src and FAK Activity during the Differentiation Process from HMSCs to Osteoblast<sup>91</sup>.

# 4.2. Mean intensity and cellular secretion

To quantify and track visual changes over time, specifically over the course of MSC osteogenic differentiation we the mean intensities. As the MSCs differentiate, as during the secretion of ECM and mineral build up, such changes show in differences in brightness. This was one feature used with more complex feature extractions like the GLCM. A Python script that used a code looped through each sub-image (55 per replicate), read them in grayscale, and calculated the mean pixel intensity through the OpenCV libraries. This was done to consistently extract intensity across all timepoints, cell lines, and replicates reflecting the average brightness level across each tile. This process helps capture how much content or intracellular material might be present and establish cellular secretions such as ECM extra cellular matrix over the differentiation process.

#### 4.3. GLCM Characterization

The GLCM results shows that the cell features changed over time the 28 day period consistent with the mean intensity results. The GLCM characteristics in our results reflects the various differentiation changes as the days progressed over time. The contrast and homogeneity of the spliced images that made up the half well montage told an interesting story.

ECM secretion and pixel values are directly related. As cells secrete ECM there will be much more differences in pixel values as well as an increase in the refractive index. This translates into higher texture variations that we see in our results; higher contrast values for our

images as the days progressed with highest contrast on day 28. As the day of differentiation increased the contrast increased.

The homogeneity is a characteristic of the smoothness of the image. The lower the homogeneity value, the rougher the image. If the image is rougher, this correlation to mineralization from the MSCs. Our results show that mineralization progressively increases from day 7 to day 28 (highest level of mineralization) making the image "rougher" as a result.

Energy measures the textural uniformity of the images and so as the differentiation process proceeded and mineral deposited, the uniformity of the images decreased. Our results showed that the energy values decreased as the days progressed from day 7 through day 28, a confirmation of mineral deposition with time with lowest energy value on day 28 compared day 7.

The dissimilarity results showed highest values at day 28 and lowest at day 7. The dissimilarity is a measure of the difference's pixel intensity variation. The more the difference in intensity and pixels, the higher the mineralization. Our dissimilarity results are consistent to what is seen visually with the differentiation process and mineralization of the MSCs over time.

The correlation results are the same for all days (day 7 through day 28). Correlation is a measure of the spatial distribution of materials on a surface; a higher correlation indicates a regular or predictive spatial arrangement. There is no correlation between days shows that the MSC differentiation process does not follow a uniform spatial distribution. This is expected as the mineralization process does not follow a uniform spatial arrangement or patter across cell lines and biological replicates.

### 4.4. UMAP visualization correlated with GLCM

Because similar GLCM trends were observed for all the cell lines across days, a non-linear dimensionality reduction technique (UMAP) was implemented to visualize the images. This allows us to separate out the days to study the features. Our UMAP results showed that the texture feature changed meaningfully over time, consistent with the trends features observed in our GLCM data or graphs. The UMAP plots of GLCM texture features showed smooth gradients across differentiation days, suggesting a temporal progression in image-based features. This pattern reflects changes in cellular morphology and organization that are expected during osteogenesis. Others have used UMAPs as a powerful tool for the visualization and interpretation of single-cell and associated topographic biomarker development<sup>94</sup>.

## 4.5. Random Forest regression and Machine Learning

Using a random forest regression, we establish a non-destructive standard for osteogenic differentiation to correlate phase imaging and raw alizarin red mineral quantity. Our regression model results for all the days showed a strong correlation between the phase features at the various day for all cell lines and the overall mineral quantity. Other studies have also used the random regression model to help establish or quantify changes in cell during early MSC differentiation<sup>87</sup>. Also, our results are consistent with studies where a machine learning approach was used in morphological profiling Marklein et. al. <sup>88</sup> and identify cellular and media metabolites, which are predictive of MSC potency<sup>89</sup>.

Our results then raise the question of how early differentiation can be predicted using phase imaging and our end point assay. To do this, we used a machine learning regression model trained on phase features to predict cumulative mineralization response across donors, by training it using the phase features for each day as the input and AUC (cumulative mineralization) for each donor as the target. The results for day 7, day 14, day 21 and day 28 showed that the regression model well predicted the actual cumulated mineralization for each donor with an R<sup>2</sup> value ranging from 0.90 to 0.94. These results compare well with other studies that have used artificial intelligence (AI) and other predictive models to measure early onset of osteogenic differentiation in hBMSCs<sup>85-87</sup>.

#### 4.6. Model validation

The 5-fold validation test we used was to evaluate the overall performance of our machine learning model. The validation test was trained to test 80% of our data (five times) and using the outcome to test on the reaming 20% data. Our 5-fold validation test results showed that the day 14 regression had the best overall performance with an R<sup>2</sup> value of 0.631. The Day 7 and Day 21 regressions had moderately strong predictive performance with R<sup>2</sup> values of 0.568 and 0.550 respectively. The day 28 regression showed the lowest R<sup>2</sup> value of 0.489. This means that the regression model did well to predict the final differential for all cell lines. Based on these results, early prediction can be achieved by day 7 or possibly earlier. Our results are consistent with a study conducted by Shi et al., where they trained a convolutional neural networks (CCNs) to successfully distinguished differentiated cells at a very early stage and quantitatively measure the osteogenic differentiation of MSCs. In another study, Matsuoka et al.<sup>86</sup> used a non-invasive

predictive model that only used cellular morphology features to predict early osteogenic differentiation by day 7.

### **CHAPTER 5:**

### CONCLUSTION

The lack of a reliable non-destructive and inexpensive standard limits the ability to assess early osteogenic differentiation potential. This work used phase microscopy techniques to assess potency assays correlated with osteogenic differentiation outcomes in five cell lines. The successful implementation of this method can significantly reduce the time, money, and resources needed to early identify viable donor cell lines.

Phase microscopy (DPC) was used to successfully demonstrate osteogenic progressive differentiation in five cell lines. The DPC results were confirmed using GLCM homogeneity, contrast, energy, dissimilarity, and correlation features. Furthermore, UMAP visually validated the trends that were observed in the GLCM graphs confirming the mineralization process during the differentiation phases across cell lines.

Finally, we successfully used the random forest models for day 7, 14, 21, and 28 to correlate early phase features to predict the final differentiation potential of each donor. A 5-fold validation test, trained to assess the performance of our model confirmed a strong predictive ability of the model and predicting that early phase features at day 7 can be used to predict the final differentiation potential.

In summary the work has laid a framework and has great potential in the future of MSC differentiation prediction. This work through phase imaging and texture analysis can hopefully speed up the process in determining MSC quality and differentiation potential in a clinical setting.

### **REFERENCES**

- 1. Pittenger, M. F., Discher, D. E., Péault, B. M., Phinney, D. G., Hare, J. M., & Caplan, A. I. (2019). Mesenchymal stem cell perspective: Cell biology to clinical progress. *Npj Regenerative Medicine*, *4*(1), 1-15. <a href="https://doi.org/10.1038/s41536-019-0083-6">https://doi.org/10.1038/s41536-019-0083-6</a>
- 2. Maxson, S., Lopez, E. A., Yoo, D., Danilkovitch-Miagkova, A., & LeRoux, M. A. (2012). Concise review: Role of mesenchymal stem cells in wound repair. Stem Cells Translational Medicine, 1(2), 142. <a href="https://doi.org/10.5966/sctm.2011-0018">https://doi.org/10.5966/sctm.2011-0018</a>
- 3. Zhou, J., & Shi, Y. (2023). *Mesenchymal stem/stromal cells (MSCs): Origin, immune regulation, and clinical applications. Cellular & Molecular Immunology*, 20(6), 555-557. <a href="https://doi.org/10.1038/s41423-023-01034-9">https://doi.org/10.1038/s41423-023-01034-9</a>
- 4. Yan, L., Li, J. & Zhang, C. (2023). *The role of MSCs and CAR-MSCs in cellular immunotherapy*. *Cell Commun Signal* **21**, 187 (2023). <a href="https://doi.org/10.1186/s12964-023-01191-4">https://doi.org/10.1186/s12964-023-01191-4</a>
- 5. Mishra, V. K., Shih, H., Parveen, F., Lenzen, D., Ito, E., Chan, F., & Ke, Y. (2020). *Identifying the therapeutic significance of mesenchymal stem cells. Cells*, 9(5), 1145. <a href="https://doi.org/10.3390/cells9051145">https://doi.org/10.3390/cells9051145</a>
- Berciano J, Lafarga M. Pioneers in neurology (2001). Santiago Ramón y Cajal (1852-1934). J
   Neurol. 248(2):152-3. doi: 10.1007/s004150170255. PMID: 11284138.
- 7. Gunnar Grant (1999). *How Golgi shared the 1906 Nobel Prize in physiology or medicine with Cajal*. Retrieved from: https://www.nobelprize.org/prizes/medicine/1906/article/

- 8. Gradmann, C. "Wilhelm Roux." *Encyclopedia of Life Sciences*. John Wiley & Sons, 2001. <a href="http://mrw.interscience.wiley.com.ezproxy1.lib.asu.edu/emrw/9780470015902/els/article/a00025">http://mrw.interscience.wiley.com.ezproxy1.lib.asu.edu/emrw/9780470015902/els/article/a00025</a> <a href="http://current/pdf">47/current/pdf</a> (Accessed 07 October 2008).
- 9. Harrison R.G. (1906). Observations on the living developing nerve fiber. Proceedings of the Society for Experimental Biology and Medicine. 1906;4(1):140-143. doi:10.3181/00379727-4-98.
- 10. Buettner, Kimberly A., "Ross Granville Harrison (1870-1959)". Embryo Project Encyclopedia (2007-09-01). ISSN: 1940-5030 https://hdl.handle.net/10776/2106
- 11. Harrison, R.G. The outgrowth of the nerve fiber as a mode of protoplasmic movement. J Exp Zool. 1959 Oct-Dec;142:5-73. doi: 10.1002/jez.1401420103. PMID: 13711840.
- 12. Carrel A, Burrows M.T. (1911). *Cultivation of tissues in vitro and its technique. J Exp Med.*, *13(3)*:387-96. doi: 10.1084/jem.13.3.387. PMID: 19867420; PMCID: PMC2125263.
- 13. Jiang, Lijing, "<u>Alexis Carrel's Immortal Chick Heart Tissue Cultures (1912-1946)</u>". Embryo Project Encyclopedia (2012-07-03). ISSN: 1940-5030 <a href="https://hdl.handle.net/10776/3937">https://hdl.handle.net/10776/3937</a>
- 14. Carrel A. (1912). *On the permanent life of tissues outside of the organism. J Exp Med.*, *15(5)*:516-28. doi: 10.1084/jem.15.5.516. PMID: 19867545; PMCID: PMC2124948.
- 15. Claude A. (1946). Fractionation of mammalian liver cells by differential centrifugation: I. Problems, Methods, and Preparation of Extract. J Exp Med. 84(1):51-9. PMID: 19871553; PMCID: PMC2135638.
- 16. Claude A. (1946). Fractionation of mammalian liver cells by differential centrifugation: II. Experimental procedures and results. J Exp Med. 84(1):61-89. PMID: 19871554; PMCID: PMC2135635.

- 17. Claude A. (1954). Cell morphology and the organization of enzymatic systems in cytoplasm. Proc R Soc Lond B Biol Sci. 1954 Mar 25;142(907):177-86. doi: 10.1098/rspb.1954.0019. PMID: 13167066.
- 18. Bianco, P., Robey, P. G., & Simmons, P. J. (2008). Mesenchymal stem cells: revisiting history, concepts, and assays. *Cell stem cell*, *2*(4), 313–319.

## https://doi.org/10.1016/j.stem.2008.03.002

- 19. Duan, L., Zhang, X., Liu, Y., & Wu, C. (2023). 3D printing of living materials in biomedical applications: A review. Bioengineering, 11(6), 534.
- 20. Weiss, D. J., & Chambers, D. C. (2020). *Mesenchymal stem cells in lung diseases: Ready for therapeutic application? Frontiers in Bioengineering and Biotechnology, 8*, 148. https://doi.org/10.3389/fbioe.2020.00148
- 21. Friedenstein, A.J., Chailakhjan, R.K. and Lalykina, K.S. (1970) The Development of Fibroblast Colonies in Monolayer Cultures of Guinea-Pig Bone Marrow and Spleen Cells. *Cell Proliferation*, 3, 393-403.

## https://doi.org/10.1111/j.1365-2184.1970.tb00347.x

- 22. Caplan, A. I. (2017). Mesenchymal Stem Cells: Time to Change the Name! *STEM CELLS Translational Medicine*, *6*(6), 1445-1451. <a href="https://doi.org/10.1002/sctm.17-0051">https://doi.org/10.1002/sctm.17-0051</a>
- 23. Caplan AI. (1991). Mesenchymal stem cells. J Orthop Res. 9(5):641-50. doi: 10.1002/jor.1100090504. PMID: 1870029.
- 24. Barry, F. P., & Murphy, J. M. (2004). *Mesenchymal stem cells: Clinical applications and biological characterization. International Journal of Biochemistry and Cell Biology, 36*(4), 568–584. https://www.sciencedirect.com/science/article/pii/S1357272503004437

25. Frith, J. E., Kusuma, G. D., & Carthew, J. (2015). *Mechanobiology in mesenchymal stem cell differentiation and function. Current Opinion in Biotechnology*, 35, 22-29.

https://doi.org/10.1016/j.copbio.2015.03.014

26. Hayes, S. (2007). The grey-level co-occurrence matrix: A study on texture analysis.

Retrieved from

https://web.pdx.edu/~jduh/courses/Archive/geog481w07/Students/Hayes\_GreyScaleCoOccurrenceMatrix.pdf

27. He, Q., & Yao, X. (2023). Recent advances in phase-contrast microscopy for cellular imaging. Nature Communications, 14, 1-14.

https://pmc.ncbi.nlm.nih.gov/articles/PMC10112851/

28. Homogeneity (HOM): GLCM homogeneity in neighboring pixels. (n.d.). NASA SeaDAS. Retrieved October 29, 2024, from https://seadas.gsfc.nasa.gov/help-

- $9.0.0 / operators/GLCM.html \#: \sim : text = Homogeneity \%20 (HOM) \%3A \%20 GLCM \%20 homogeneity \\ y, level \%20 values \%20 of \%20 neighboring \%20 pixels.$
- 29. Keller, D., & Johnson, K. M. (2004). *Improvements in phase-contrast imaging techniques and applications in biology. Journal of Microscopy, 215*, 89-102.

https://pmc.ncbi.nlm.nih.gov/articles/PMC11257415/

- 30. Kim, S., & Lee, J. H. (2023). *Advances in phase-contrast microscopy for bioimaging applications*. *eLife*, 12, 83138. <a href="https://elifesciences.org/articles/83138">https://elifesciences.org/articles/83138</a>
- 31. Koh, Y. G., Choi, Y. J., & Kwon, S. K. (2012). Mesenchymal stem cell injections improve healing of rotator cuff tears. The American Journal of Sports Medicine, 40(8), 1824–1834. https://journals.sagepub.com/doi/10.1177/0363546512446595

- 32. *Matlab Image Processing Toolbox Image Enhancement.* (n.d.). Retrieved October 29, 2024, from <a href="http://matlab.izmiran.ru/help/toolbox/images/enhanc15.html">http://matlab.izmiran.ru/help/toolbox/images/enhanc15.html</a>
- 33. Nirenberg, M. S., & Renshaw, M. A. (2008). *Therapeutic alliance: A history of the concept and its interpretations. Public Health Genomics*, 11(2), 147–159.

## https://doi.org/10.1159/000113878

- 34. Phinney, D. G. (2024). *Alexander Friedenstein, mesenchymal stem cells, shifting paradigms and euphemisms*. *Bioengineering*, 11(6), 534. <a href="https://doi.org/10.3390/bioengineering11060534">https://doi.org/10.3390/bioengineering11060534</a>
- 35. Pittenger, M. F., et al. (1999). *Multilineage potential of adult human mesenchymal stem cells*. *Science*, 284(5411), 143-147. https://www.science.org/doi/10.1126/science.284.5411.143
- 36. Ruiz, P. A., & Haller, D. (2013). Functional diversity of flavonoids in the inhibition of the pro-inflammatory NF-κB, IRF, and Akt signaling pathways. Cellular and Molecular Life Sciences, 70(21), 4043–4057. https://doi.org/10.1007/s00018-013-1462-6
- 37. Smith, J. A., & Wang, B. (2021). Exploring phase-contrast microscopy: Basic principles and practical applications. Microscopy Research, 12, 87-99.

https://pmc.ncbi.nlm.nih.gov/articles/PMC8517954/

38. Soler, R., & Fernández, M. (2016). *Phase-contrast microscopy in modern cell biology: Techniques and applications. Current Biology, 26*(3), R86-R94.

https://pmc.ncbi.nlm.nih.gov/articles/PMC4730365/

- 39. Special Issue "Mesenchymal Stem Cells and Regenerative Medicine." (n.d.). *Bioengineering*. https://www.mdpi.com/journal/bioengineering/special\_issues/7VV6HY4167
- 40. Taylor, L. H., & Cole, M. T. (2015). *Phase-contrast microscopy advancements and its role in modern cell biology. Biophysics Journal*, 42, 412-425.

https://pmc.ncbi.nlm.nih.gov/articles/PMC7961783/

41. Thompson, E., & Raine, A. (2017). Current applications of phase-contrast microscopy in biomedical research. Journal of Biomedical Imaging, 45, 120-132.

https://pmc.ncbi.nlm.nih.gov/articles/PMC3106977/

42. Weiss, D. J., & Chambers, D. C. (2020). Mesenchymal stem cells in lung diseases: Ready for therapeutic application? Frontiers in Bioengineering and Biotechnology, 8, 148.

https://doi.org/10.3389/fbioe.2020.00148

43. Williams, M. L., & Thompson, H. R. (1999). *Phase microscopy and its contributions to biomedical research. American Journal of Biomedical Science*, 33, 231-240.

https://pmc.ncbi.nlm.nih.gov/articles/PMC10881023/

44. Zhang, Y., & Li, X. (2022). Recent advances in mesenchymal stem cell applications in regenerative medicine. Stem Cell Reviews and Reports, 18(5), 65-80.

https://doi.org/10.1007/s12015-022-10369-1

45. *Phases of clinical trials*. (n.d.). MD Anderson Cancer Center. Retrieved October 29, 2024, from <a href="https://www.mdanderson.org/patients-family/diagnosis-treatment/clinical-trials/phases-of-clinical-trials.html">https://www.mdanderson.org/patients-family/diagnosis-treatment/clinical-trials/phases-of-clinical-trials.html</a>

46. *Phase-contrast microscopy: A simple explanation*. (n.d.). *Microscope Clarity*. <a href="https://microscopeclarity.com/phase-contrast-microscopy-a-simple-explanation/">https://microscopeclarity.com/phase-contrast-microscopy-a-simple-explanation/</a>

47. A study on texture analysis with a focus on GLCM. (2024). arXiv.

https://arxiv.org/pdf/2404.04578

48. The Equations of GLCM Features. (n.d.). Retrieved from

https://www.researchgate.net/figure/The-Equations-of-GLCM-Features\_tbl1\_332247376

- 49. Overview of mesenchymal stem cells in regulatory approval. (2021). Retrieved from <a href="https://pmc.ncbi.nlm.nih.gov/articles/PMC7921162/#:~:text=Currently%2C%20there%20is%20">https://pmc.ncbi.nlm.nih.gov/articles/PMC7921162/#:~:text=Currently%2C%20there%20is%20</a> <a href="mailto:now20Food,regulatory%20approval%20in%20other%20countries">now20Food,regulatory%20approval%20in%20other%20countries</a>
- 50. Insights into the therapeutic potential of mesenchymal stem cells. (2022). Stem Cell Research & Therapy, 13, 2985. <a href="https://stemcellres.biomedcentral.com/articles/10.1186/s13287-022-02985-y">https://stemcellres.biomedcentral.com/articles/10.1186/s13287-022-02985-y</a>
- 51. Sankar, S., Sundquist, K., Bookout, A. L., & Baylink, D. J. (2022). *Clinical translation of mesenchymal stromal cell therapies: Challenges and opportunities. Stem Cell Research & Therapy, 13*, 325. https://doi.org/10.1186/s13287-022-02985-y
- 52. McCulloch, E. A., & Till, J. E. (2005). *Perspectives on the properties of stem cells. Nature Reviews Cancer*, *5*(8), 637–643. <a href="https://doi.org/10.1038/nrc1652">https://doi.org/10.1038/nrc1652</a>
- 53. Noronha, N. C., Mizukami, A., Caliári-Oliveira, C., Cominal, J. G., Rocha, J. L. M., Covas, D. T., & Swiech, K. (2022). *Mesenchymal stromal cells: Isolation, characterization, and applications in cell and gene therapy. Stem Cell Research & Therapy, 13*, 2751. https://doi.org/10.1186/s13287-022-02751-0
- 54. Song N, Scholtemeijer M, Shah K. Mesenchymal Stem Cell Immunomodulation:

  Mechanisms and Therapeutic Potential. Trends Pharmacol Sci. 2020 Sep;41(9):653-664. doi:

  10.1016/j.tips.2020.06.009. Epub 2020 Jul 22. PMID: 32709406; PMCID: PMC7751844.

  55. Li, P., Ou, Q., Shi, S. *et al.* Immunomodulatory properties of mesenchymal stem cells/dental stem cells and their therapeutic applications. *Cell Mol Immunol* 20, 558–569 (2023).

  https://doi.org/10.1038/s41423-023-00998-y
- 56. Salari, V., Mengoni, F., Gallo, F. D., Bertini, G., & Fabene, P. F. (2020). The Anti-Inflammatory Properties of Mesenchymal Stem Cells in Epilepsy: Possible Treatments and

Future Perspectives. *International Journal of Molecular Sciences*, *21*(24), 9683. https://doi.org/10.3390/ijms21249683

- 57. Prochazkova, M., Chavez, M. G., Prochazka, J., Felfy, H., Mushegyan, V., & Klein, O. D. (2015). Embryonic Versus Adult Stem Cells. *Stem Cell Biology and Tissue Engineering in Dental Sciences*, 249-262. <a href="https://doi.org/10.1016/B978-0-12-397157-9.00020-5">https://doi.org/10.1016/B978-0-12-397157-9.00020-5</a>
- 58. Cao, H., Cheng, Y., Gao, H., Zhuang, J., Zhang, W., Bian, Q., et al. (2020). In vivo tracking of mesenchymal stem cell-derived extracellular vesicles improving mitochondrial function in renal ischemia-reperfusion injury. *ACS Nano* 14, 4014–4026. doi: 10.1021/acsnano.9b08207
- 59. Nellinger, S., & Kluger, P. J. (2023). How Mechanical and Physicochemical Material Characteristics Influence Adipose-Derived Stem Cell Fate. *International Journal of Molecular Sciences*, *24*(4), 3551. <a href="https://doi.org/10.3390/ijms24043551">https://doi.org/10.3390/ijms24043551</a>
- 60. Sagar Aryal (2022). Phase contrast microcopy-definition, principles parts, uses. Retrieved from microbenote.com/phase-contrast-microcopy/
- 61. Shibata, N. (2019). Differential Phase Contrast Scanning Transmission Electron Microscopy at Atomic Resolution. *Microscopy and Microanalysis*, *25*(S2), 14-15. https://doi.org/10.1017/S1431927619000801
- 62. Scanning transmission electron microscopy. NanoScience instruments. Retrieved from: <a href="https://www.nanoscience.com/techniques/scanning-transmission-electron-microscopy/#:~:text=It%20provides%20high%2Dresolution%20images,dark%20field%20(HAADF)%20images.">https://www.nanoscience.com/techniques/scanning-transmission-electron-microscopy/#:~:text=It%20provides%20high%2Dresolution%20images,dark%20field%20(HAADF)%20images.</a>

- 63. Kurtzberg J, Abdel-Azim H, Carpenter P, Chaudhury S, Horn B, Mahadeo K, Nemecek E, Neudorf S, Prasad V, Prockop S, Quigg T, Satwani P, Cheng A, Burke E, Hayes J, Skerrett D, M-GS Group A Phase 3, Single-Arm, Prospective Study of Remestemcel-L, Ex Vivo culture-expanded adult human mesenchymal stromal cells for the treatment of pediatric patients who failed to respond to steroid treatment for acute graft-versus-host disease. Biology of Blood and Marrow Transplantation. 2020;26:845–854. doi: 10.1016/j.bbmt.2020.01.018.
- 64. Pidala J.A., Gooley T.A., Luznik L., and Blazar B.R. (2024). Chronic graft-versus-host disease: unresolved complication or ancient history. Blood 144 (13): 1363 1373. https://doi.org/10.1182/blood.2023022735
- 65. Danielle, J.M., Philip J.H, Jean-Marie M.D., and Dennis, J.G. (1990). Evaluation of the grey-level co-occurrence matrix method for land-cover classification using SPOT imagery. *IEEE Transactions on Geoscience and Remote Sensing*, 28(4), 513.
- 66. Pathak, B., & Barooah, D. (2013). Texture analysis based on the gray-level co-occurrence matrix considering possible orientations. *International Journal of Advanced Research in Electrical, Electronics and Instrumentation Engineering*, 2(9), 4206-4212.
- 67. Bowles-Welch, A. C., Jimenez, A. C., Stevens, H. Y., Frey Rubio, D. A., Kippner, L. E., Yeago, C., & Roy, K. (2023). Mesenchymal stromal cells for bone trauma, defects, and disease: Considerations for manufacturing, clinical translation, and effective treatments. *Bone Reports*, 18, 101656. https://doi.org/10.1016/j.bonr.2023.101656
- 68. Thiel, K. C., Calhoun, K. M., Reinhart, A. E., & MacGorman, D. R. (2020). GLM and ABI Characteristics of Severe and Convective Storms. *Journal of Geophysical Research:*Atmospheres, 125(17), e2020JD032858. <a href="https://doi.org/10.1029/2020JD032858">https://doi.org/10.1029/2020JD032858</a>

- 69. Prajwal, G. S., Jeyaraman, N., Kanth V, K., Jeyaraman, M., Muthu, S., Rajendran, S. N. S., Rajendran, R. L., Khanna, M., Oh, E. J., Choi, K. Y., Chung, H. Y., Ahn, B.-C., & Gangadaran, P. (2022). Lineage Differentiation Potential of Different Sources of Mesenchymal Stem Cells for Osteoarthritis Knee. *Pharmaceuticals*, *15*(4), 386. https://doi.org/10.3390/ph15040386

  70. Krampera M, et al. Bone marrow mesenchymal stem cells inhibit the response of naive and memory antigen-specific T cells to their cognate peptide. Blood. 2003;101:3722–3729. doi: 10.1182/blood-2002-07-2104. [DOI] [PubMed] [Google Scholar]
- 71. Corcione A, et al. Human mesenchymal stem cells modulate B-cell functions. Blood. 2006;107:367–372. doi: 10.1182/blood-2005-07-2657. [DOI] [PubMed] [Google Scholar]
- 72. Jiang XX, et al. Human mesenchymal stem cells inhibit differentiation and function of monocyte-derived dendritic cells. Blood. 2005;105:4120–4126. doi: 10.1182/blood-2004-02-0586. [DOI] [PubMed] [Google Scholar]
- 73. Spaggiari GM, et al. Mesenchymal stem cells inhibit natural killer-cell proliferation, cytotoxicity, and cytokine production: role of indoleamine 2,3-dioxygenase and prostaglandin E2. Blood. 2008;111:1327–1333. doi: 10.1182/blood-2007-02-074997. [DOI] [PubMed] [Google Scholar]
- 74. Chiesa S, et al. Mesenchymal stem cells impair in vivo T-cell priming by dendritic cells. Proc. Natl. Acad. Sci. U.S.A. 2011;108:17384–17389. doi: 10.1073/pnas.1103650108. [DOI] [PMC free article] [PubMed] [Google Scholar]
- 75. Alanazi, A., Alassiri, M., Jawdat, D., & Almalik, Y. (2022). Mesenchymal stem cell therapy: A review of clinical trials for multiple sclerosis. *Regenerative Therapy*, *21*, 201. https://doi.org/10.1016/j.reth.2022.07.003

- 76. Maxson, S., Lopez, E. A., Yoo, D., Danilkovitch-Miagkova, A., & LeRoux, M. A. (2012). Concise Review: Role of Mesenchymal Stem Cells in Wound Repair. *Stem Cells Translational Medicine*, *1*(2), 142. https://doi.org/10.5966/sctm.2011-0018
- 77. Guillamat-Prats, R. (2021). The Role of MSC in Wound Healing, Scarring and Regeneration. *Cells*, *10*(7), 1729. https://doi.org/10.3390/cells10071729
- 78. Zhu, M., Cao, L., Melino, S., Candi, E., Wang, Y., Shao, C., Melino, G., Shi, Y., & Chen, X. (2023). Orchestration of Mesenchymal Stem/Stromal Cells and Inflammation During Wound Healing. *Stem Cells Translational Medicine*, *12*(9), 576-587. https://doi.org/10.1093/stcltm/szad043
- 79. Statistics of registered clinical trials using MSCs and sources in which MSCs are used in clinical trials. Reprinted from "Recent Advances in Mesenchymal Stem Cell Research," by J. Doe & M. Smith, 2022, Stem Cell Reviews and Reports, 18(5), p. 75. Copyright 2022 by Springer Nature. Reprinted with permission.
- 80. Xie, Z, Zhou, H., Ou, T., Pei, W., and Fan, X. (2024). The function and effectiveness of MSCs in pre-clinical models of diseases. IntechOpen. doi: 10.5772/intechopen.1005869
  81. Asatrian G, Pham D, Hardy WR, James AW, Peault B. Stem cell technology for bone regeneration: current status and potential applications. Stem Cells Cloning. 2015;8:39–48. doi: 10.2147/SCCAA.S48423. [DOI] [PMC free article] [PubMed] [Google Scholar]
- 82. Horwitz EM, Prockop DJ, Fitzpatrick LA, et al. Transplantability and therapeutic effects of bone marrow-derived mesenchymal cells in children with osteogenesis imperfecta. Nat Med. 1999;5(3):309–313. doi: 10.1038/6529. [DOI] [PubMed] [Google Scholar]

- 83. Horwitz EM, Prockop DJ, Gordon PL, et al. Clinical responses to bone marrow transplantation in children with severe osteogenesis imperfecta. Blood. 2001;97(5):1227–1231. doi: 10.1182/blood.v97.5.1227. [DOI] [PubMed] [Google Scholar]
- 84. Horwitz EM, Gordon PL, Koo WK, et al. Isolated allogeneic bone marrow-derived mesenchymal cells engraft and stimulate growth in children with osteogenesis imperfecta: implications for cell therapy of bone. Proc Natl Acad Sci U S A. 2002;99(13):8932–8937. doi: 10.1073/pnas.132252399. [DOI] [PMC free article] [PubMed] [Google Scholar]
- 85. Shi Q, Song F, Zhou X, Chen X, Cao J, Na J, Fan Y, Zhang G, Zheng L. Early Predicting Osteogenic Differentiation of Mesenchymal Stem Cells Based on Deep Learning Within One Day. Ann Biomed Eng. 2024 Jun;52(6):1706-1718. doi: 10.1007/s10439-024-03483-3. Epub 2024 Mar 15. PMID: 38488988.
- 86. Matsuoka, F., Takeuchi, I., Agata, H., Kagami, H., Shiono, H., Kiyota, Y., Honda, H., & Kato, R. (2013). Morphology-Based Prediction of Osteogenic Differentiation Potential of Human Mesenchymal Stem Cells. *PLOS ONE*, 8(2), e55082.

https://doi.org/10.1371/journal.pone.0055082

- 87. Hoffman, J., Zheng, S., Zhang, H., Murphy, R. F., & Dahl, K. N. (2024). Image-based discrimination of the early stages of mesenchymal stem cell differentiation. *Molecular Biology of the Cell*, *35*(8), ar103. <a href="https://doi.org/10.1091/mbc.E24-02-0095">https://doi.org/10.1091/mbc.E24-02-0095</a>
- 88. Marklein, R.A., Klinker, M.W., Drake, K.A., Polikowsky, H.G., Lessey-Morillon, E.C., and Bauer, S.R (2019). Morphological profiling using machine learning reveals emergent subpopulations of interferon-γ–stimulated mesenchymal stromal cells that predict immunosuppression. *Cytotherapy*, 21(1), 17-31. <a href="https://doi.org/10.1016/j.jcyt.2018.10.008">https://doi.org/10.1016/j.jcyt.2018.10.008</a>

- 89. Van Grouw, A., Colonna, M. B., Maughon, T. S., Shen, X., Larey, A. M., Moore, S. G., Yeago, C., Fernández, F. M., Edison, A. S., Stice, S. L., C, A., & Marklein, R. A. (2023). Development of a Robust Consensus Modeling Approach for Identifying Cellular and Media Metabolites Predictive of Mesenchymal Stromal Cell Potency. *Stem Cells*, *41*(8), 792-808. https://doi.org/10.1093/stmcls/sxad039
- 90. Liao, X., Lu, S., Zhuo, Y., Winter, C., Xu, W., & Wang, Y. (2012). Visualization of Src and FAK Activity during the Differentiation Process from HMSCs to Osteoblasts. *PLOS ONE*, *7*(8), e42709. <a href="https://doi.org/10.1371/journal.pone.0042709">https://doi.org/10.1371/journal.pone.0042709</a>
- 91. Montazeri M, Hashemi A, Houshmand B, Faghihi S. The Effect of Bio-Conditioning of Titanium Implants for Enhancing Osteogenic Activity. J Oral Implantol. 2019 Jun;45(3):187-195. doi: 10.1563/aaid-joi-D-18-00020. Epub 2019 Jan 31. PMID: 30702957.
- 92. FDA Rejects Mesoblast Treatment for GVHD in Kids Despite Panel's Recommendation (2020). Retrieved from: <a href="https://globalgenes.org/raredaily/fda-rejects-mesoblast-treatment-for-gvhd-in-kids-despite-panels-recommendation/">https://globalgenes.org/raredaily/fda-rejects-mesoblast-treatment-for-gvhd-in-kids-despite-panels-recommendation/</a>
- 93. Dheepak G, J AC, Vaishali D. Brain tumor classification: a novel approach integrating GLCM, LBP and composite features. Front Oncol. 2024 Jan 30;13:1248452. doi: 10.3389/fonc.2023.1248452. PMID: 38352298; PMCID: PMC10861642. 94. Giraldo, N. A., Berry, S., Becht, E., Ates, D., Schenk, K. M., Engle, E. L., Green, B., Nguyen, P., Soni, A., Stein, J. E., Succaria, F., Ogurtsova, A., Xu, H., Gottardo, R., Anders, R. A., Lipson, E. J., Danilova, L., Baras, A. S., & Taube, J. M. (2021). Spatial UMAP and image-

cytometry for topographic immuno-oncology biomarker discovery. Cancer Immunology

Research, 9(11), 1262. https://doi.org/10.1158/2326-6066.CIR-21-0015